University of Pardubice
Faculty of Chemical Technology

Malonic Acid Derivatives as Acceptor Parts of Push-Pull Chromophores

DISSERTATION
(Annotation)

2017 Ing. Milan Klikar

CONTENTS

1. INTRODUCTION

Organic push-pull chromophores currently constitute intensively investigated class of π-conjugated systems, which has found many applications across chemistry and material sciences.[1] The unique and peculiar properties of push-pull molecules such as color, (hyper)polarizability, dipolar character, and extraordinary linear and nonlinear optical behavior, etc. are mainly induced by intramolecular charge transfer (ICT) from the electron donor via π-linker to the electron acceptor.[2] Optical properties, HOMO-LUMO gap, dipole moments, hyperpolarizabilty coefficients, etc. are mainly dictated by the extent of the ICT. In push-pull molecules, the aforementioned fundamental properties can easily be tuned by the type of used electron donors and acceptors, length and composition of the π-linker, and overall chromophore arrangement.[3] High importance of D-π-A systems can clearly be demonstrated by their wide applications as active substances in organic electronics, molecular optics,[4] and semiconductors.[5]

Malonic acid (MA) was prepared for the first time by oxidation of malic acid by French chemist V. Dessaignes already in 1858.[6] Since this early experiment, malonic acid and its derivatives became well-known and widely studied class of organic compounds. They are extensively used in industry, especially in pharmaceuticals, agrochemicals, vitamins, dyes, adhesives, and fragrances.[7] A common feature of MA derivatives is high reactivity of the central methylene bridge. Due to acidity of the CH_2, induced by two neighboring carbonyl groups, these compounds easily undergo alkylation, arylation, aldol and Knoevenagel condensations, and MA derivatives are also often utilized in the construction of heterocycles.[8] Knoevenagel condensation is one of the main synthetic tools used for introducing MA derivatives into the structure of push-pull chromophores. This reaction between a carbonyl compound and a substance bearing active methylene group is generally acid- or base-catalyzed.[9]

For many decades, MA derivatives have widely been used as electron withdrawing parts of push-pull chromophores. Their popularity can be ascribed to their commercial availability, low price, easy incorporation into the chromophore, and relatively high electron withdrawing character. Moreover, a right choice of MA derivative enables facile fine-tuning of target chromophore properties. According to the functional groups, MA derivatives can be divided into three general subgroups: i) *nitriles* (e.g. cyanoacetic acid, ethyl cyanoacetate, and malondinitrile, ii) *esters* (e.g. dialkyl malonate and Meldrum´s acid), and iii) *imides* (e.g. (thio)barbituric acid). Malonic acid and cyanoacetic acid are currently privileged precursors

for the construction of chromophores for DSSC (dye-sensitized solar cell).[10] The principal advantage of cyanoacetic acid can be seen in combining both withdrawing (-CN) and anchoring (-COOH) abilities. Malondinitrile, as a starting compound for the formation of dicyanovinyl (DCV) withdrawing unit, is one of the most popular electron acceptor ever. For instance, DCV unit has extensively been studied by Diederich et al.[11] and recently reviewed by our working group.[12] On the contrary, dialkyl malonates have rarely been employed in the construction of push-pull chromophores.[13] It is probably due to its weak withdrawing ability caused by +M effects of alkoxy groups. Meldrum´s acid as a cyclic ester of malonic acid is likewise scarcely used in push-pull chromophores, but it was used in some D-π-A systems so far.[14] On the other hand, barbituric acid and its thio analogue are very popular MA derivatives with noticeable withdrawing strength. These acceptor moieties abundantly occurs in many (mero)cyanine dyes,[15] nonlinear optic chromophores,[16] solvatochromic[17] and near-infrared probes[18] and supramolecular complexes based on multiple H-bonding interactions.[19]

1.1 Malonic acid derivatives as electron-withdrawing units in push-pull molecules

In 2013, our group has utilized *N*,*N*´-dibutylbarbituric acid as powerful and well-soluble acceptor moiety of push-pull chromophores with systematically elongated π-linker.[20] This preceding research inspired me to study and critically compare withdrawing abilities of acceptor units based on various MA derivatives. It is quite surprising that, to the best of my knowledge, no attempts have been made to systematically compare withdrawing strength of wide range of malonic derivatives. Beside pure MA derivatives, this study also involves two additional 1,3-diketo analogues such as dimedone and indan-1,3-dione. Whereas dimedone, representing an analogue of Meldrum´s acid, was used very scarcely in organic (opto)electronics,[21] indan-1,3-dione proved to be a very powerful acceptor, for instance in our recent T-shaped chromophores.[22] The electron withdrawing abilities of the particular MA-derivatives can roughly be estimated according to their pK_a values.

Based on the 2-(*N*-piperidinyl)thiophene central donor, 32 model push-pull molecules (31 new) with systematically varied malonic acid-derived peripheral acceptors have been designed and prepared. Further property tuning has been achieved by modifying the π-linker and the structural arrangement (linear vs. branched D-π-A systems). Malonic acid derivatives such as cyanoacetic acid (CAA), malondinitrile (MDN), diethyl malonate (DEM), Meldrum´s acid (MEL), and *N*,*N*´-dibutyl(thio)barbituric acid (DBB and DBTB) as well as 1,3-diketo analogues dimedone (DMD) and indan-1,3-dione (IND) were employed as acceptor moieties.

According to structural features, all target chromophores **A1–A8** can be divided in four subseries **a**–**d**. The chromophore number specifies type of the acceptor(s): **1** = CAA, **2** = MDN, **3** = DEM, **4** = MEL, **5** = DMD, **6** = DBB, **7** = DBTB, and **8** = IND. Labels **a**–**d** indicates length of the π-linker (ethenylene in series **a** and **c**; but-1,3-dienylene in series **b** and **d**) as well as degree of branching (linear **a** and **b**; branched **c** and **d**), see *Fig. 1*. Withdrawing abilities of malonic acid acceptors were examined both by experiment including X-ray analysis, differential scanning calorimetry, electrochemistry, and UV-Vis absorption spectroscopy and by DFT calculations. Based on the measured and calculated data, thorough structure-property relationships have been elucidated and discussed.

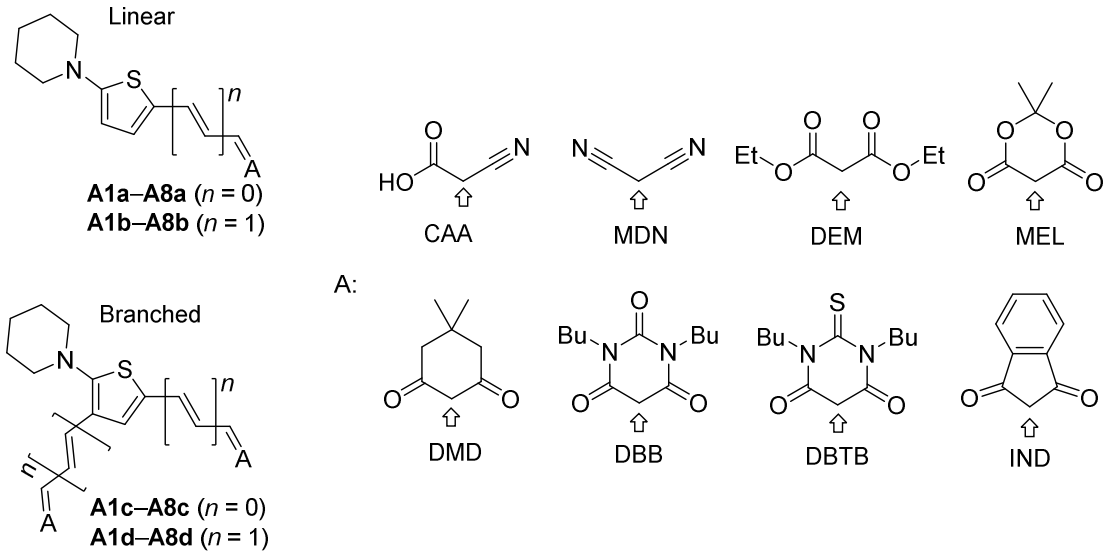

Figure 1. *Target linear/branched chromophores **A1–A8** with eight withdrawing units based on MA derivatives and its analogues.*

1.2 Multipodal arrangement of push-pull chromophores

Compared to inorganic materials, a dominant advantage of organic push-pull systems can be seen in their facile and relatively inexpensive/manifold synthesis, well-defined structure, and tunable (opto)electronic properties. The latter property tuning of fundamental parameters such as the position of the longest-wavelength absorption maxima, the HOMO-LUMO gap, and the dipole moment as well as solubility and thermal stability can be achieved through a variation of the particular part of the D-π-A system (π-linker, donor, acceptor, arrangement, planarity etc.).[3]

With respect to donor group, *N*,*N*-dialkylamino unit is considered as one of the most efficient electron releasing group used for the construction of linear push-pull molecules.[11a, 22b, 23] Higher multipodal chromophore arrangements such as quadrupolar and octupolar are achieved on di- or triphenylamine (DPA and TPA) donors. These central

electron releasing moieties equipped with peripheral MDN or barbituric acceptors showed to be very powerful charge-transfer chromophores exhibiting strong absorption and emission in the visible/near IR region of the spectra, solvatochromic behavior, narrowed HOMO-LUMO gap, and noticeable nonlinearities. These features predestinate them as fluorophores for OLEDs, 2PA absorbers, ion sensors, and probes for bio-imaging. [24]

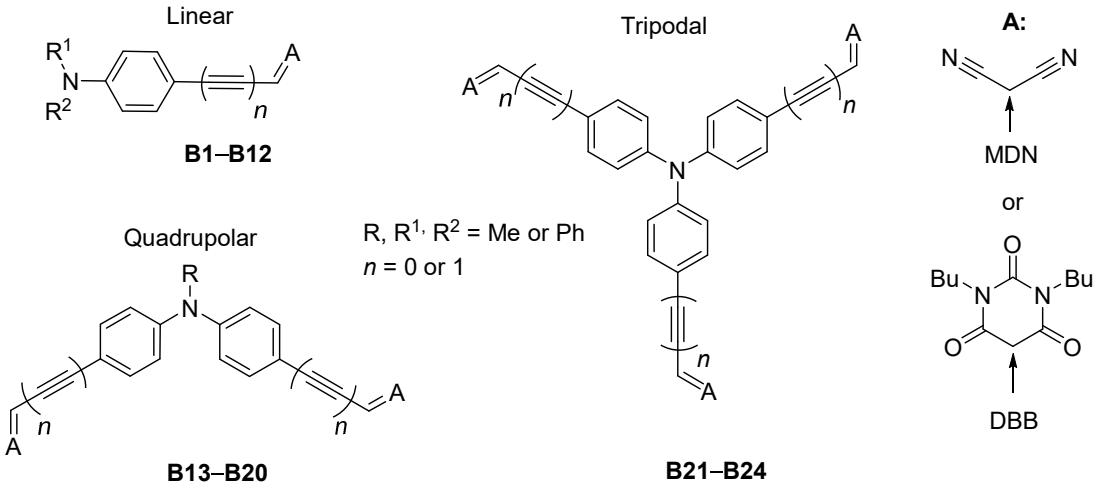

Figure 2. *Target molecules **B1–B24** with linear, quadrupolar, and tripodal arrangements.*

Recently, our research group focused on model tripodal push-pull molecules containing TPA central donor with various peripheral cyano withdrawing units. This study clearly demonstrates a strong withdrawing ability of MDN unit compared to other used cyano acceptors. Moreover, these molecules showed remarkable nonlinear optical properties, two-photon absorption (2PA) in particular.[25] Within these initial studies on very popular TPA derivatives, I have also preliminarily focused on a branching effect. According to the current state of the art, not much attention has been devoted to a comparison of push-pull molecules with linear, quadrupolar, and tripodal arrangements built on an identical *N*,*N*-dialkyl(aryl)anilino donor.[26]

For these reasons, I have decided to perform a complex study that compares fundamental properties of gradually branched push-pull molecules derived from TPA and its amino analogues. Twentyfour (16 new) model push-pull chromophores **B1**–**B24** (*Fig. 2*) with systematically altered structure were designed, synthesized, and further investigated to thoroughly elucidate structure-property relationships. These chromophores **B1**–**B24** possess systematically extended π-conjugated system, altered acceptor, and increased degree of branching (multipodality). Whereas *N*,*N*-dialkyl(aryl)anilines were used as electron donors, malononitrile MDN and *N,N´*-dibutylbarbituric acid DBB act as electron withdrawing moieties.

According to the structural features of chromophores **B1–B24**, we can divide them into the following sub-groups:

- chromophores with **MDN** (odd numbers) or **DBB** (even numbers) acceptor unit,
- chromophores with (**B3**, **B4**, **B7**, **B8**, **B11**, **B12**, **B15**, **B16**, **B19**, **B20**, **B23**, **B24**) or without (**B1**, **B2**, **B5**, **B6**, **B9**, **B10**, **B13**, **B14**, **B17**, **B18**, **B21**, **B22**) additional acetylenic spacer linked to the acceptor,
- chromophores with various degree of branching: linear (**B1–B12**), quadrupolar (**B13–B20**), and tripodal (**B21–B24**).

In addition, linear **B1–B12** and quadrupolar molecules **B13–B20** possess systematically varied substituents appended to the amino donor (Me or Ph), which would also affect the donor strength and overall extension of the π-system. The impact of these structural changes in **B1–B24** were investigated by electrochemistry, UV/Vis absorption spectra, and differential scanning calorimetry. The photoinduced piezooptics, a parametrical third order nonlinear optical effect, was also studied. The aforementioned experimental data were further completed with the results from DFT calculations.

2. EXPERIMENTAL

2.1 Malonic acid derivatives as electron-withdrawing units in push-pull molecules

In general, all target push-pull chromophores **A1–A8** were prepared via Knoevenagel condensation. Cyanoacetic acid (CAA), malondinitrile (MDN), diethyl malonate (DEM), Meldrum´s acid (MEL), dimedone (DMD), and indan-1,3-dione (IND) are commercially available. The remaining acceptor precursors, namely *N,N´*-dibutylbarbituric acid **DBB** and *N,N´*-dibutyl-2-thiobarbituric acid **DBTB** were synthesized via acid/base catalyzed condensation of *N,N´*-dibutyl(thio)ureas **3** and **6** with malonic acid **4** or diethyl malonate **DEM** according to *Scheme 1*.

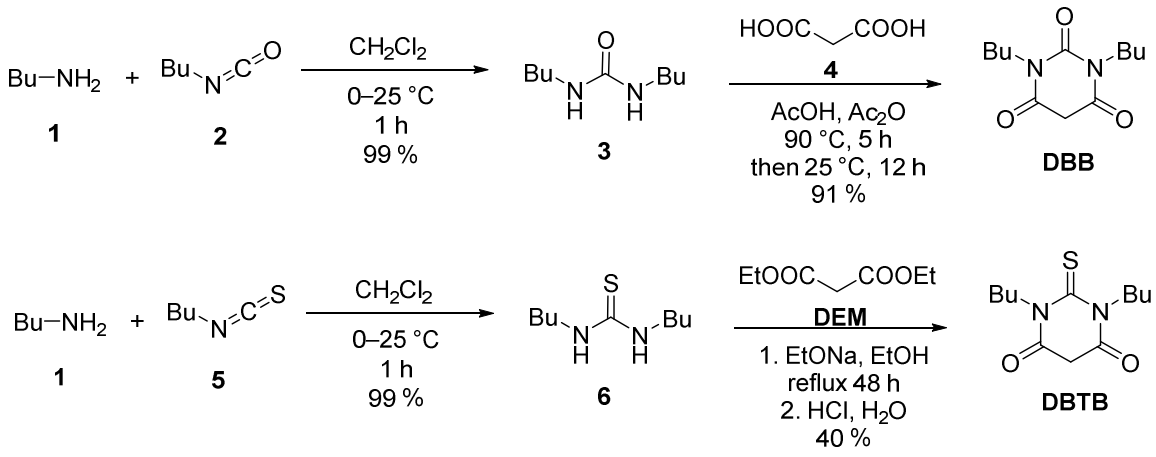

Scheme 1. *Synthesis of N,N´-dibutyl(thio)barbituric acids **DBB** and **DBTB**.*

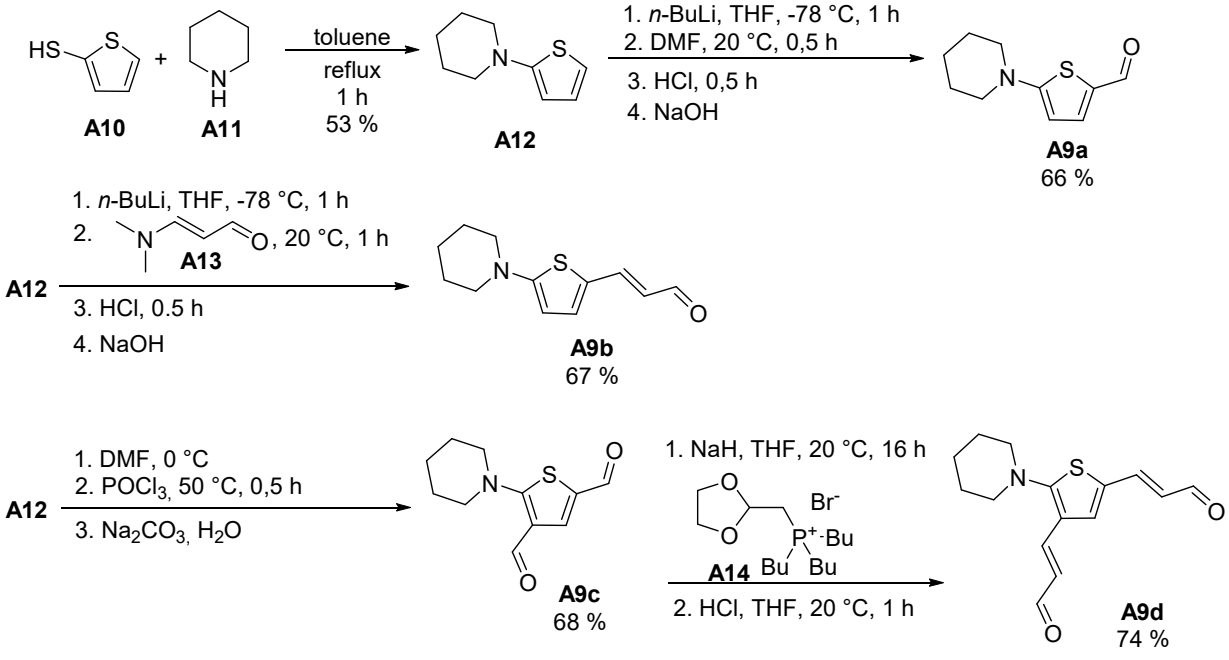

Scheme 2. *Construction of PIT aldehydes **A9a–d**.*

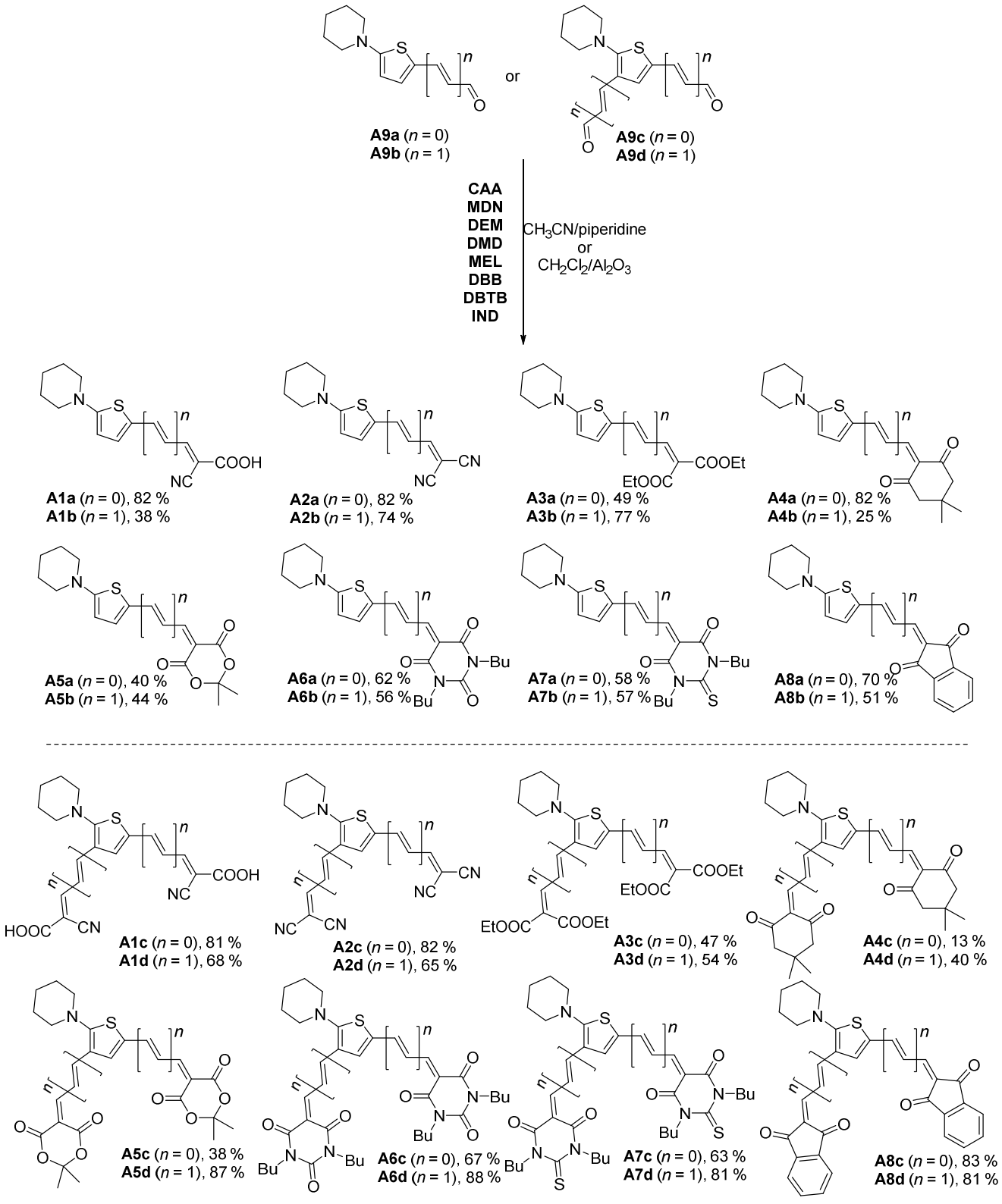

Scheme 3. *General synthetic pathway towards chromophores **A1–A8** via Knoevenagel condensation.*

Scheme 2 shows overall preparations of PIT aldehydes **A9a–d**. 2-(*N*-Piperidinyl)thiophene PIT (**A12**), as a fundamental D/π building block, was prepared by the reaction of thiophene-2-thiol **A10** with piperidine **A11** with 53% yield.[27] Its direct

lithiation with *n*-BuLi at −78 °C and subsequent reaction with DMF afforded linear aldehyde **A9a** with 66% yield.[28] A similar reaction sequence with 3-(*N,N*-dimethylamino)acrolein **A13** afforded extended aldehyde **A9b** with 67% yield. PIT also underwent Vilsmeier-Haack formylation with DMF/$POCl_3$ system.[29] In contrast to available reports,[28, 29] I have isolated only dialdehyde **A9c** regardless of the used amount of DMF/$POCl_3$. This twofold formylation provided branched dialdehyde **A9c** in satisfactory yield of 68 %. However, all attempts to perform similar Vilsmeier-Haack formylation of **A12** with **A13** resulted in very exothermic reaction and decomposition. Hence, extended dialdehyde **A9d** was prepared via alternative twofold Wittig elongation of **A9c** using commercially available phosphonium salt **A14**.[28] Subsequent hydrolysis of the formed diacetal intermediate yielded **A9d** with 74% yield.

With PIT aldehydes **A9a–d** in hand, I have carried out their Knoevenagel condensations with aforementioned MA derivatives (*Scheme 3*). As the particular MA derivatives exhibit various basicity/nucleophilicity and aldehydes **A9a–d** possess different reactivity/electrophilicity, the reaction conditions had to be optimized. In some reactions, a generally well-working and very convenient CH_2Cl_2/Al_2O_3 system[30] had to be replaced by CH_3CN/piperidine one. The Knoevenagel reactions of **A9a–d** with parent malonic acid provided completely insoluble compounds. The attained yields do not show any noticeable trends, they rather represent an intersection of acid-base properties of the starting materials as well as the used separation techniques.

2.2 Multipodal arrangement of push-pull chromophores

In general, target compounds **B1–B24** were prepared by two general pathways. The synthesis of chromophores with less extended π-linker without triple bond(s) utilizes aromatic aldehydes **B41–B46**. Whereas aldehydes **B41** and **B43–B46** are commercially available, aldehyde **B42** was prepared from the methyldiphenylamine **B26**. Its iodination using $I_2/AgNO_3$ system[31] afforded both mono and diiododiphenylamines **B29** and **B30**. This inseparable mixture was further subjected to lithiation with *n*-BuLi at −78 °C and subsequent formylation with DMF providing **B42** in 80% yield. The simultaneously formed aldehyde **B43** was discarded as a by-product (*Scheme 4*). The pairs of chromophores **B1/B2, B5/B6, B9/B10, B13/B14, B17/B18,** and **B21/B22** were prepared via Al_2O_3 catalyzed[30] Knoevenagel condensation of aldehydes **B41–B46** with malondinitrile **MDN** or *N,N´*-dibutylbarbituric acid **DBB** in satisfactory yields 42–94 % (*Scheme 5*). This facile reaction sequence provided twelve variously arranged chromophores with two terminal malonic acceptors.

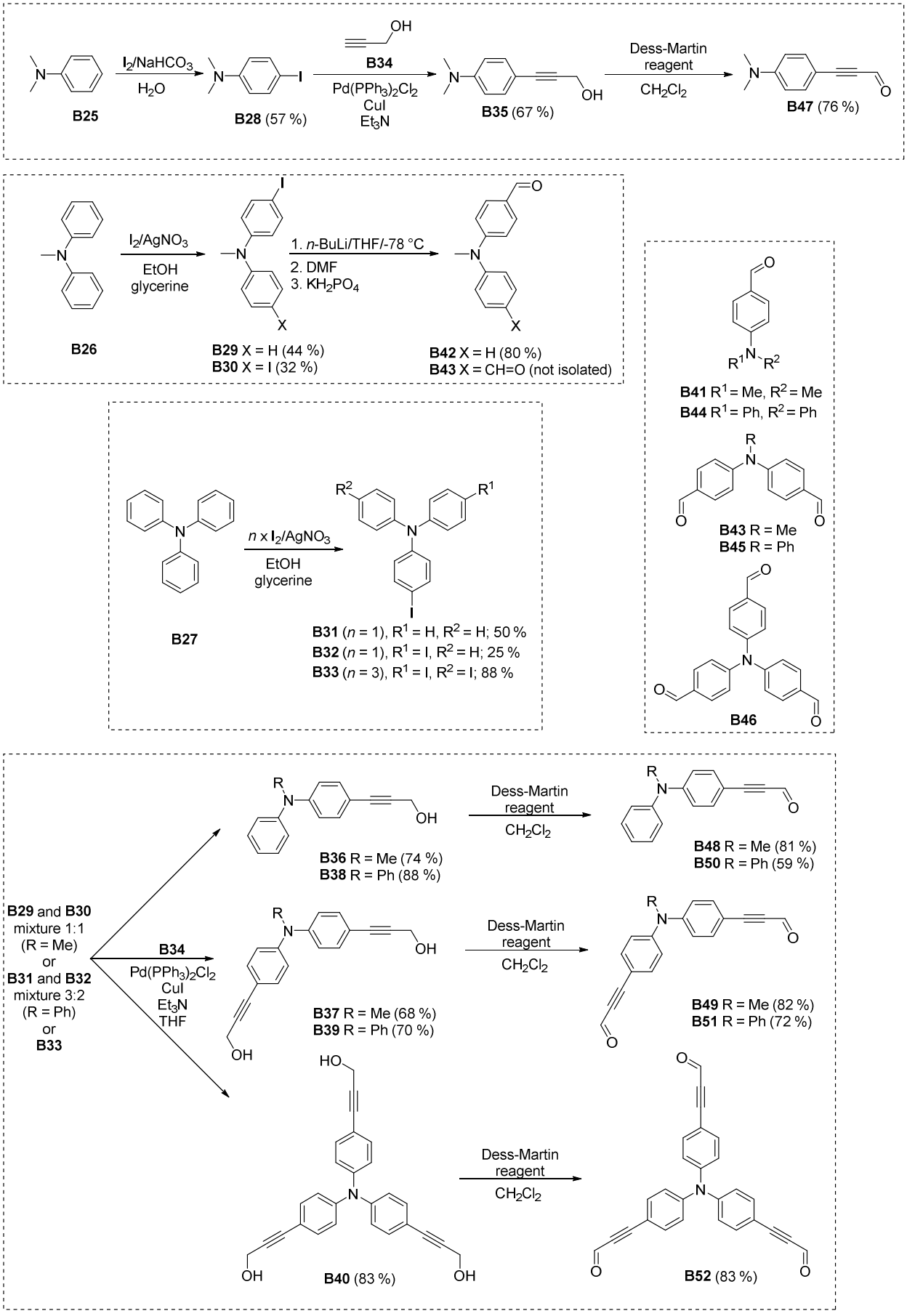

Scheme 4. *Synthetic pathways towards desired aldehydes* ***B42*** *and* ***B47–B52****.*

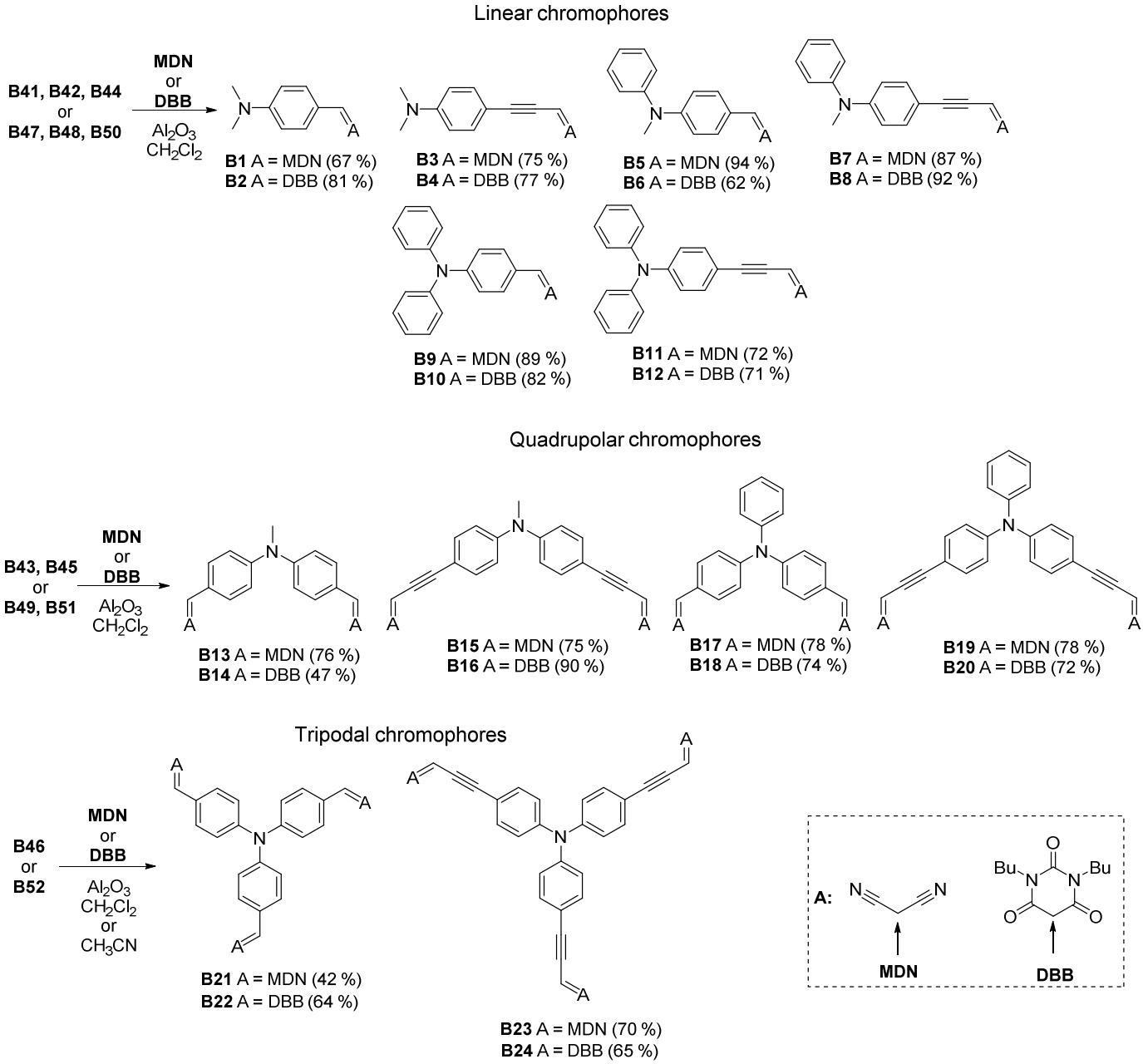

Scheme 5. *Final Knoevenagel condensation giving target chromophores **B1–B24**.*

The synthesis of chromophores **B3/B4, B7/B8, B11/B12, B15/B16, B19/B20, B23/B24** bearing an additional acetylenic spacer started with preparation of extended aldehydes **B47–B52** (*Scheme 4*). These aldehydes were synthesized by Sonogashira cross-coupling of the corresponding iodo derivatives **B28–B33** with propargyl alcohol **B34**. Iodination of alkyl(aryl)amines **B25–B27** with $I_2/AgNO_3(NaHCO_3)$ system[31, 32] afforded compounds **B28–B33** in reasonable yields. The degree of iodination was controlled by the amount of I_2 used. Similarly to **B29–B30**, mono and diiodotripehnylamines **B31–B32** were obtained as inseparable mixtures, which however smoothly underwent Sonogashira reaction with **B34** under standard catalytic conditions [$Pd(PPh_3)_2Cl_2$, CuI, and Et_3N][33] to afford alcohols

B35–B40 in the yields of 68–70 %. All prepared alcohols **B35-B40** were easily separable by column chromatography and could be subsequently oxidized to aldehydes **B47–B52** in 59–83% yields by using Dess-Martin reagent. [34] The final step was again Al_2O_3 catalyzed Knoevenagel condensation with **MDN** or **DBB** providing all remaining chromophores. It should be noted, that Knoevenagel reaction on extended aldehydes **B47–B52** proved to be facile and gave generally higher yields than the reaction on arylaldehydes **B41–B46**.

3. RESULTS AND DISCUSSION

3.1 Malonic acid derivatives as electron-withdrawing units in push-pull molecules

3.1.1 X-ray analysis

Crystals of PIT aldehydes **A9a–Ad** as well as target chromophores **A2c**, **A4a**, **A5b**, and **A8a–b** suitable for X-ray analysis were obtained by slow diffusion of hexane into its dichloromethane solution. The ORTEP plots of PIT aldehydes as well as target chromophores are shown in *Figure 3* and *Figure 4*, respectively. These plots confirm the proposed molecular structures as well as arrangement of the particular aldehyde/chromophore in the solid state. The ORTEP plot of **A9c** further confirms observed twofold Vilsmeier-Haack formylation taking place selectively at the C3 and C5 positions of the PIT.

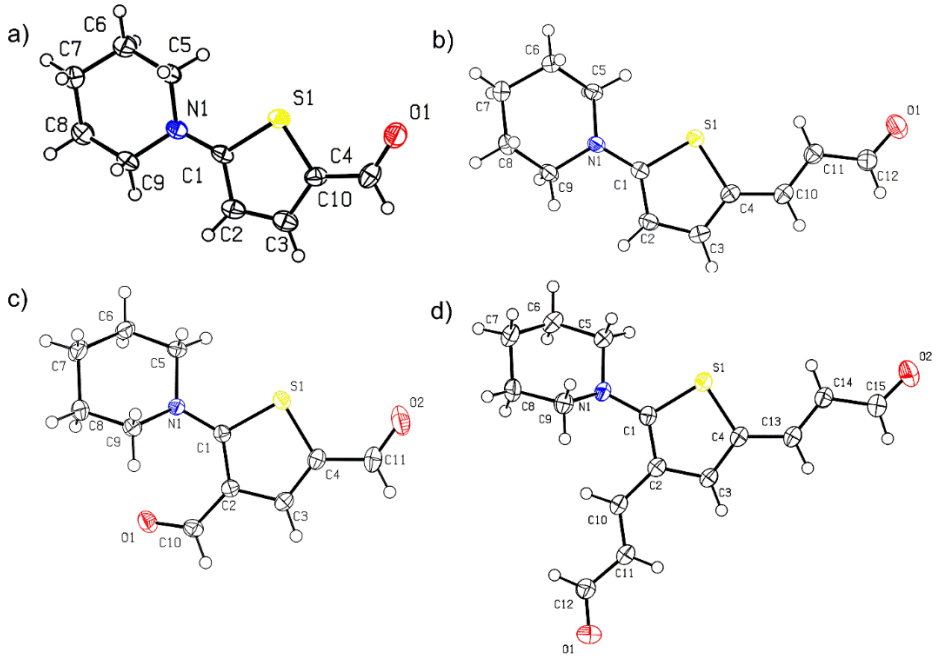

Figure 3. *X-ray molecular representations of PIT aldehydes **A9a** (a), **A9b** (b), **A9c** (c), and **A9d** (d).*

The MA-derived acceptor units in **A2c**, **A4a**, **A5b**, and **A8a–b** are almost perfectly co-planar with the central thiophene moiety. Regardless of the used π-linker (ethenylene or but-1,3-dienylene), the dihedral angles between these two moieties do not exceed 10 ° (generally 1–3 °). This allows efficient overlap of the π-electron clouds across the whole π-system and facilitates the ICT between the donor and the acceptor. Branching of the chromophore caused only minor deviation of the piperidine ring.

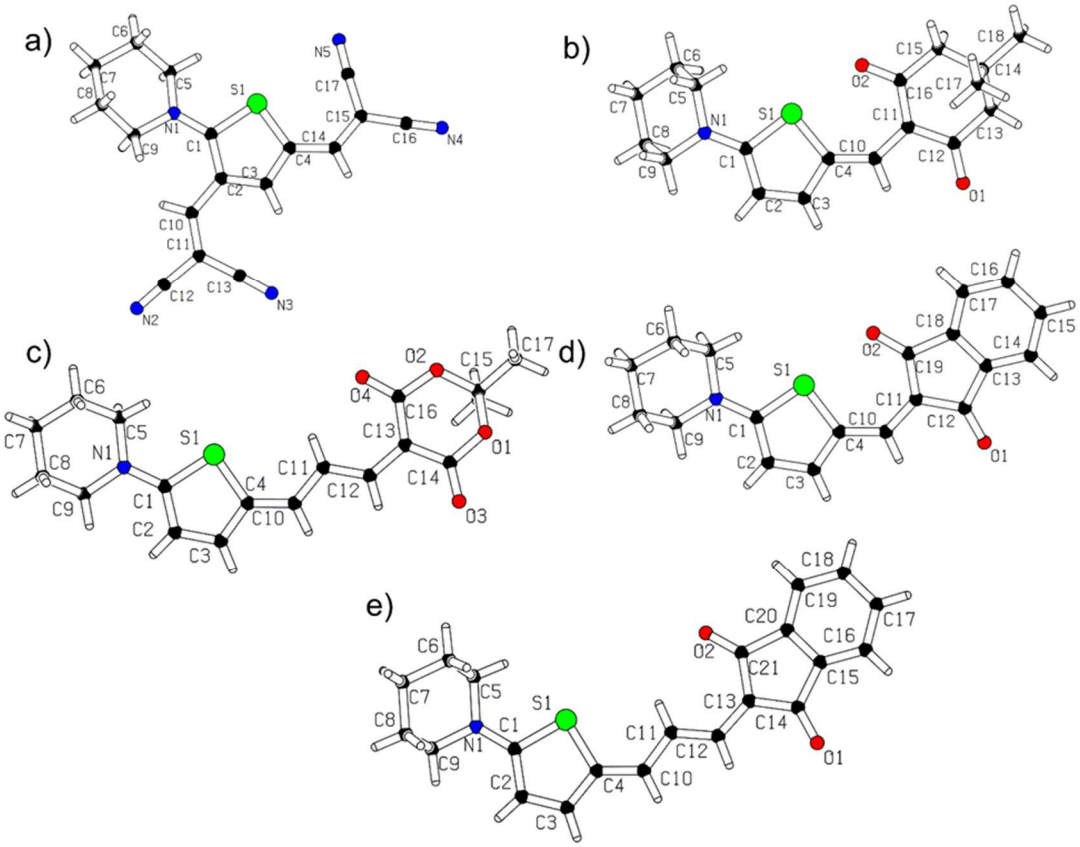

Figure 4. *X-ray molecular representations of chromophores **A2c** (a), **A4a** (b), **A5b** (c), **A8a** (d), and **A8b** (e).*

A variation of the C-C bond distances within the thiophene ring in a range from typical C=C double bond to ca 1.42 Å has been revealed from the X-ray data. This can be attributed to elongated thiophene bonds, while the rest of the C–C, C–N and C–O (multiple) bonds are localized at appropriate places with lengths similar to the literature values. In this respect, the extent of the ICT can be assessed by calculating bond length alternation within the central thiophene ring. Its quinoid character/aromaticity can easily be determined by the Bird index I_5.[35] Whereas the Bird index of unsubstituted thiophene equals to 66, thiophene rings in **A2c**, **A4a**, **A5b**, and **A8a–b** possess I_5 within the range of 59 to 63. This implies less aromaticity and higher quinoid character of the thiophene rings due to the ICT. The supramolecular arrangement of **A2c**, **A4a**, **A5b**, and **A8a–b** reveals 2D-layered array structures due to extensive π-π stacking supported by numerous non-covalent C–H···negative atom interactions.

3.1.2 Thermal properties

Thermal behaviour of compounds **A1–A8** was studied by differential scanning calorimetry (DSC). *Figure 5* shows thermograms of representative compounds **A7a–d** (DBTB chromophores) while *Table 1* lists all measured melting points (T_m) and temperatures of thermal

decompositions (T_d). The measured melting points range from 62 to 261 °C. The temperature of decomposition was estimated within the range of 171–303 °C.

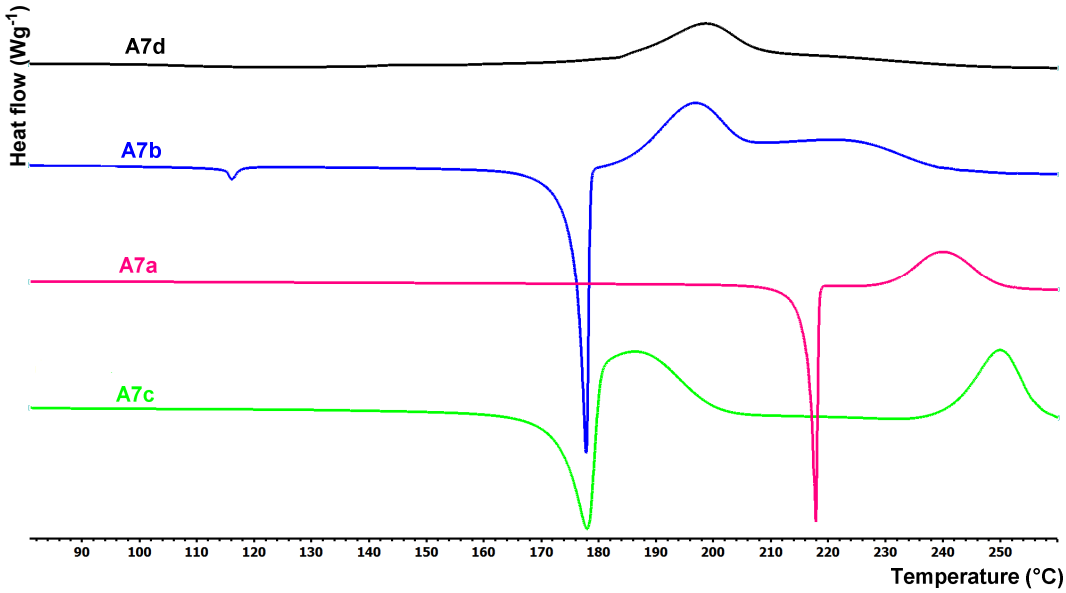

Figure 5. *Representative DSC curves of compounds **A7a–d** (DBTB chromophores) determined with a scanning rate of 3 °C/min under inert atmosphere of N_2.*

Except **1a**, all linear chromophores in series **a** exhibited very sharp endothermic peak of melting. Chromophore **3a** is viscous oil, which decomposed directly at 269 °C followed by a melting of the decomposed residue. For **A4a** and **A7a**, the exothermic peaks of decomposition were observed shortly after melting, while **A1a**, **A2a**, **A5a**, **A6a**, and **A8a** were stable in liquid phase for additional 40–150 °C above their melting point. Except **A3b** bearing DEM acceptor unit (T_m = 62 °C), very sharp peaks of melting were found for compounds in series **b** (T_m = 155–213 °C). In contrast to **A1b–A3b**, and **A6b**, decomposition of **A4b**, **A5b**, **A7b**, and **A8b** followed immediately their melting. On the other hand, the compounds in branched series **c** and **d** showed complex thermal behaviour. Molecules **A2c** and **A6c** exhibited sharp melting peaks followed by gradual decomposition, while the melting of **A4c**, **A5c**, **A7c**, and **A8c** was immediately overset to exothermic decompositions. For most compounds in series **c** the subsequent decomposition peaks were observed as well. Oily **A3c** exhibited similar thermal behavior as **A3a**. Whereas **A2d** and **A5d** decomposed immediately after melting, **A6d** and especially **A3d** were stable also in liquid phase. On the contrary, compounds **A1d**, **A4d**, **A7d**, and **A8d** decomposed directly without melting. Desorption of the residual/crystalline solvents were observed for compounds **A1b**, **A1c**, **A1d**, **A5b**, **A6d**, and **A8d**. Moreover, **A5c** and **A6d** also showed solid-solid transitions at 125 and 140 °C, respectively.

From the measured thermal properties, we can conclude the following outcomes:

- Elongation of the π-linker by embedding an additional double bond decreases T_d (e.g. linear series **b** vs. **a**; *Figure 5*).
- The measured T_d values are very close (ΔT_d = 5–40 °C) for pairs of compounds with the same acceptors in series **c** and **d** (*Figure 5*).
- In general, the linear compounds **A1a–A8a** and **A1b–A8b** always showed melting peaks, whereas the branched **A1c–A8c** and **A1d–A8d** often underwent additional thermal processes or decomposed directly without melting.
- The lowest melting points were determined for **A3b** (62 °C) and **A3d** (123 °C) with DEM acceptor bearing ethyl chains. In general, alkyl chains hamper crystallization and significantly affect the melting points.
- On the contrary, compounds end-capped with DEM unit(s) (**A3a–d**) exhibited the highest average T_d values.
- Similarly, CAA-, MDN-, and IND-terminated compounds (**A1a–d**, **A2a–d**, and **A8a–d**) significantly resisted thermal decomposition.
- MEL-substituted **A5a–d** possess higher T_d compared to structurally similar DMD-ones **A4a–d** (effect of the oxygen atoms).
- The effect of chalcogenide atom can be distinguish between DBB (**A6a–d**) and DBTB (**A7a–d**) derivatives. The sulfur atom in DBTB increases the melting point and generally decreases T_d compared to DBB oxygen analogs.

With respect to the aforementioned conclusions, the highest melting point and decomposition temperature were observed for **A2d** (T_d = 261 °C) and **A2a** (T_d = 303 °C) end-capped with MDN acceptor unit(s).

3.1.3 Electrochemistry

Electrochemical measurements of chromophores **A1–A8** were carried out in DMF containing 0.1 M Bu_4NPF_6 in a three electrode cell by cyclic voltammetry (CV) and rotating disk voltammetry (RDV). The working electrode was glassy carbon disk (2 mm in diameter) for CV and RDV experiments. As reference and auxiliary electrodes were used saturated calomel electrode (SCE) separated by a bridge filled with supporting electrolyte and Pt wire, respectively. All potentials are given *vs.* SCE, *Table 1* lists the acquired data. Chromophores **A1a–d** with CAA acceptor(s) were not measurable by the employed electrochemical techniques.

Table 1. *Summarized thermal, electrochemical, and linear optical properties of chromophores **A1–A8**.*

Compound	T_m (°C)[a]	T_d (°C)[b]	$E_{1/2(ox1)}$ (V)[c]	$E_{1/2(red1)}$ (V)[c]	ΔE (V)[c]	E_{HOMO} (eV)[e]	E_{LUMO} (eV)[e]	λ_{max}^{A} (nm/eV)[f]	$\varepsilon_{max}^{A} \cdot 10^3$ ($M^{-1} \cdot cm^{-1}$)[f]
A1a	130	205	-[g]	-[g]	-	-	-	436/2.84, 459/2.70[h]	28.8 45.9[h]
A2a	143	303	0.95[d]	-1.29	2.24	-5.30	-3.06	464/2.67	57.9
A3a	-	269	0.72	-1.63	2.35	-5.07	-2.72	430/2.88	36.1
A4a	205	217	0.83	-1.36	2.19	-5.18	-2.99	488/2.54	81.4
A5a	184	232	0.94[d]	-1.30[d]	2.24	-5.29	-3.05	468/2.65	90.5
A6a	172	251	0.88[d]	-1.28[d]	2.16	-5.23	-3.07	486/2.55	110.6
A7a	216	231	0.94[d]	-1.15[d]	2.09	-5.29	-3.20	508/2.44	120.8
A8a	182	243	0.80	-1.21[d]	2.01	-5.15	-3.14	515/2.41	105.1
A1b	155	217	-[g]	-[g]	-	-	-	468/2.65, 533/2.33[h]	17.5 23.7[h]
A2b	155	254	0.67	-1.02	1.69	-5.02	-3.33	551/2.25	73.3
A3b	62	258	0.53	-1.33	1.86	-4.88	-3.02	466/2.66	35.2
A4b	169	179	0.59	-1.03	1.62	-4.94	-3.32	594/2.09	109.8
A5b	213	218	0.67	-0.96	1.63	-5.02	-3.39	572/2.17	142.1
A6b	148	207	0.64	-0.95	1.59	-4.99	-3.40	592/2.09	142.1
A7b	175	186	0.69	-0.82	1.51	-5.04	-3.53	614/2.02	174.9
A8b	204	215	0.56[d]	-0.93	1.49	-4.91	-3.42	619/2.00	123.0
A1c	-	264	-[g]	-[g]	-	-	-	398/3.12, 448/2.77[h]	14.7 14.1[h]
A2c	215	222	1.24	-0.92	2.16	-5.59	-3.43	472/2.63	30.3
A3c	-	298	0.96[d]	-1.45[d]	2.41	-5.31	-2.90	386/3.21	28.3
A4c	204	209	0.97	-1.02	1.99	-5.32	-3.33	497/2.49	42.7
A5c	199	205	1.15[d]	-0.90[d]	2.05	-5.50	-3.45	477/2.60	41.1
A6c	127	171	1.04[d]	-0.90	1.94	-5.39	-3.45	527/2.35	39.4
A7c	172	179	1.09[d]	-0.65	1.74	-5.44	-3.70	519/2.39	87.9
A8c	243	254	1.00	-0.85	1.85	-5.35	-3.50	556/2.23	48.3
A1d	-	250	-[g]	-[g]	-	-	-	433/2.86, 465/2.67[h]	17.8 19.1[h]
A2d	261	264	0.85	-0.85	1.70	-5.20	-3.50	522/2.38	36.8
A3d	123	286	0.71	-1.21	1.92	-5.06	-3.14	423/2.93	37.1
A4d	-	214	0.76	-0.85	1.61	-5.11	-3.50	583/2.13	29.2
A5d	235	244	0.85	-0.75	1.60	-5.20	-3.60	579/2.14	47.8
A6d	178	212	0.79	-0.75	1.54	-5.14	-3.60	598/2.07	54.8
A7d	-	184	0.85	-0.52	1.37	-5.20	-3.83	656/1.89	68.0
A8d	-	242	0.75	-0.74	1.49	-5.10	-3.61	585/2.12	43.2

[a] T_m = melting point (the point of intersection of a baseline and a tangent of thermal effect = oneset). [b] T_d = thermal decomposition (pyrolysis in N_2 atmosphere). [c] $E_{1/2(ox1)}$ and $E_{1/2(red1)}$ are half-wave potentials of the first oxidation and reduction, respectively; all potentials are given vs. SCE; $\Delta E = E_{1/2(ox1)} - E_{1/2(red1)}$. [d] Reversible process. [e] $-E_{HOMO/LUMO} = E_{1/2(ox1/red1)} + 4.429$ (Ref.[36]). [f] Measured in CH_3OH/CH_2Cl_2 24:1 at concentration 10^{-5} M. [g] Not measurable. [h] 5 µl of AcOH were added to measured solutions.

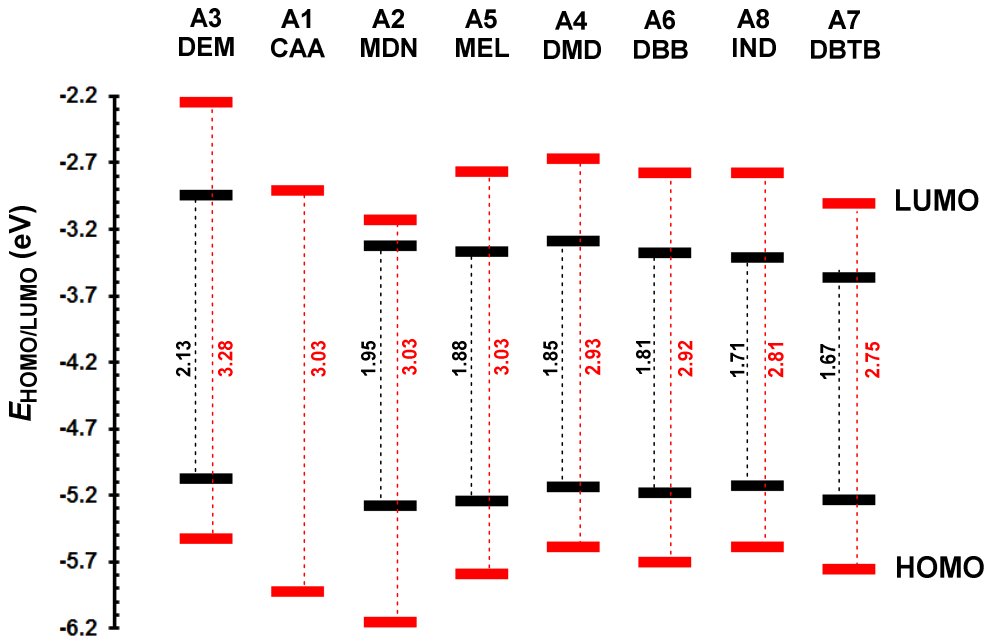

Figure 6. *Energy level diagram of averaged values of the electrochemical (**black**) and DFT calculated (**red**) energies $E_{HOMO/LUMO}$ for the particular series of MA-derived withdrawing units.*

The values of the half-wave potentials of the first oxidation and reduction $E_{1/2(ox1)}$ and $E_{1/2(red1)}$ were recorded within the range of 0.53 to 1.15 and −1.63 to −0.52 V, respectively. The first oxidation and reduction are typical one-electron processes, followed by subsequent oxidations and reductions, and are obviously a function of the number and type of the used acceptor unit(s) as well as the π-linker length (*Table 1*). Whereas the first oxidation most likely takes place at the PIT donor, the first reduction is situated on the withdrawing moiety and the adjacent π-linker. All half-wave potentials of the first oxidation and reduction were further recalculated to the energies of the HOMO and LUMO ($E_{HOMO/LUMO}$), respectively.[36] Energy level diagram of averaged values of the $E_{HOMO/LUMO}$ for the given quartet of chromophores with the same acceptor unit is shown in *Figure 6*.

As a general trend, the E_{HOMO} values gradually decreased in order **b** → **d** → **a** → **c**. Hence, extension of the π-linker shifts the HOMO levels to more positive values most significantly (**b** vs. **a** or **d** vs. **c**). Chromophore branching has the opposite effect and further reduces the E_{HOMO} values (**c** vs. **a** or **d** vs. **b**). The lowest/highest averaged HOMO level belong to chromophores **A2**/**A3** bearing MDN/DEM acceptor units. On average, the E_{LUMO} values decreased in order **a** → **b** → **c** → **d**. In contrast to the HOMO levels, the E_{LUMO} is shifted to more negative values both upon extension of the π-system and branching the chromophore. Hence, the lowest/highest averaged E_{LUMO} values were measured for chromophore **A7**/**A3** with DBTB/DEM acceptor units. As the first reduction and the LUMO are localized

on the acceptor moieties of **A1–A8**, the energies E_{LUMO} can be used to order the particular acceptor units as follows: DEM < DMD ≤ MDN ≤ MEL ≤ DBB < IND < DBTB. The difference between the first oxidation and reduction potentials/HOMO and LUMO levels (electrochemical gap, ΔE) represents a direct way for evaluating the extent of the ICT across all withdrawing units and chromophores. As the electron donating part (PIT) remained unaltered in all chromophores, the changes seen in the $E_{HOMO/LUMO}$ can be ascribed to the following structural changes:

- Length of the π-linker. Its extension always reduces the ΔE.
- Chromophore branching reduces the ΔE as well. This effect is especially pronounced when going from linear series **a** to branched series **c** and less for series **b** and **d** in which the effect of the π-linker elongation dominates.
- The HOMO-LUMO gap in **A1–A8** is mostly dictated by the withdrawing unit appended to the PIT donor. According to decreasing ΔE values, we can order the acceptor units as follows: DEM < MDN < MEL ≤ DMD < DBB < IND < DBTB (*Figure 6*).

Hence, chromophores **A7d** (1.37 eV), **A8b**, and **A8d** (both 1.49 eV) bearing DBTB and IND acceptor units possess the narrowest ΔE. On the contrary, DEM-terminated molecules **A3a** (2.35 eV) and **A3c** (2.41 eV) possess the largest HOMO-LUMO gaps.

3.1.4 One photon absorption

All target chromophores **A1–A8** are intensely colored solids or oils with a color ranging from yellow to blue, most of them showed none emissive behavior. Hence, optical absorption properties were examined by UV-Vis spectroscopy. The longest-wavelength absorption maxima λ_{max} and molar absorption coefficients ε_{max} are summarized in *Table 1*. Selected absorption spectra are shown in *Figure 7*. The longest-wavelength absorption maxima of chromophores **A1–A8** ranged from 386 to 656 nm with the corresponding ε_{max} values of $15 \cdot 10^3$ to $175 \cdot 10^3$ $M^{-1} \cdot cm^{-1}$.

Linear chromophores in series **a** and **b** exhibit always a single CT-band, whereas the spectra of branched molecules in series **c** and **d** feature two more or less developed CT-bands (*Figure 7a*). This reflects two conjugated pathways between both particular acceptors and the PIT central donor and their quadrupolar nature. According to the Frenkel exciton model, the excited state of a quadrupolar molecule is split to two bands which are energetically positioned at +V and −V (V is the inter-branch coupling) relative to the excited state

of the parent dipolar molecule.[37] For quadrupolar branched molecules are both bands one-photon allowed (observable), while the low-energy lying one possesses greater oscillator strength (larger ε_{max}). This is also the case of chromophores **A6a**/**A6c** and **A6b**/**A6d** (*Figure 7a*). For instance, **A6a** possesses one single CT-band with λ_{max} = 486 nm and ε_{max} = 110.6·10^3 M^{-1}·cm^{-1}, while the spectrum of its quadrupolar analogue **A6c** features two bands at 428 and 527 nm with ε_{max} = 24.3·10^3 and 39.4·10^3 M^{-1}·cm^{-1}, respectively. *Figure 7a* also clearly demonstrates the effect of π-linker elongation. When going from **A6a** to **A6b** or from **A6c** to **A6d** (insertion of one double bond in each branch), the positions of the longest-absorption maxima shifted bathochromically with $\Delta\lambda_{max}$ of 106 and 71 nm, respectively.

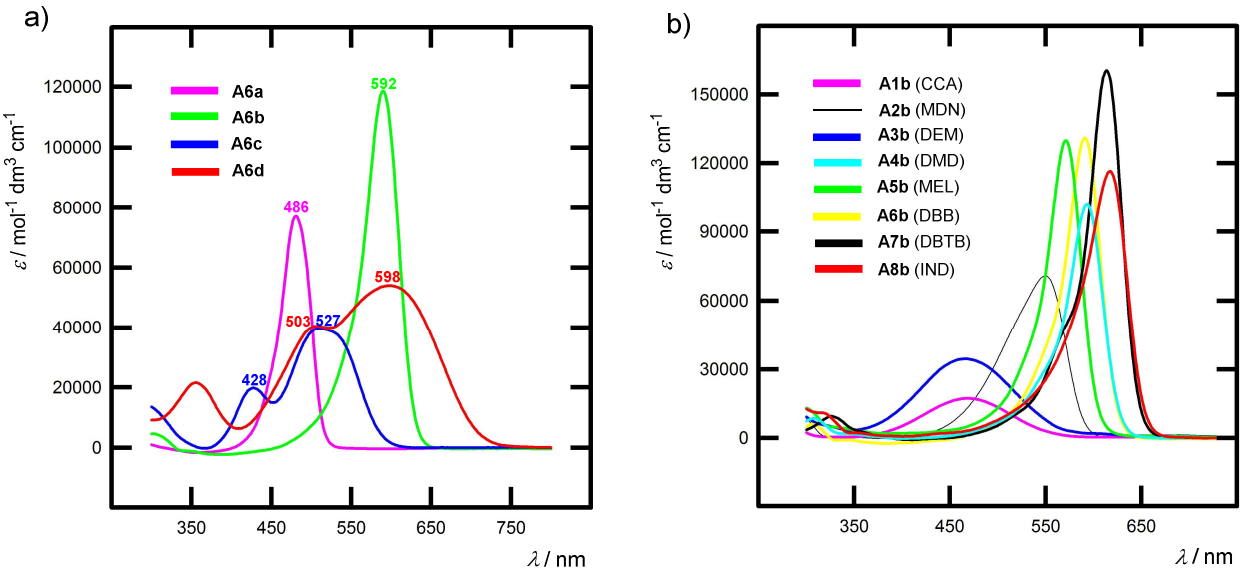

Figure 7. *Representative UV-Vis absorption spectra of DBB chromophores **A6a–d** (a) and **A1b–8d** in CH_3OH/CH_2Cl_2 (24:1) at concentration 1·10^{-5} M.*

The trends seen by electrochemical measurements are also obeyed in electronic absorption spectra. Namely, extension of the π-linker of the chromophore reduces the optical gap (1240/λ_{max}), see *Table 1*. Chromophore branching has no clear trends across the whole series as two peaks for quadrupolar chromophores in series **c** and **d** were observed. Hence, both red- and slight blue-shifts were observed (*Table 1*). Alternation of the acceptor units affects the optical properties of chromophores **A1**–**A8** most significantly. For instance, a gradual replacement of the DEM acceptor in **A3b** (λ_{max} = 466 nm) up to DBTB or IND shifted the λ_{max} to 614 (**A7b**) and 619 nm (**A8b**), respectively ($\Delta\lambda_{max}$ ~ 150 nm, *Figure 7b*). Thus, a right choice of the MA acceptor allows tuning of the optical gap by about 0.7 eV. *Figure 8* compares the averaged optical gaps of all MA derivatives. Considering the λ_{max}-derived optical gaps,

the withdrawing abilities of the particular MA derivatives showed the same trend as seen by ΔE values with the following order: DEM ≤ CAA < MDN < MEL < DMD ≤ DBB < IND ≤ DBTB. The following structure-withdrawing property relationships can be deduced among the particular MA-acceptors:

- DEM is the weakest electron acceptor, DBTB and IND are the most powerful ones.
- MDN proved to be stronger acceptor unit than CAA.
- The withdrawing behavior of CAA strongly depends on the extent of the COOH dissociation. Acidification of the media by acetic acid (*Figure 8*), resulted in significant red-shift of the spectra as the COOH remained undissociated.
- Cyclic MEL proved to be much stronger acceptor than linear DEM (lactone vs. ester). Hence, cyclic MA-derivatives are generally stronger electron acceptors.
- O→C replacement in MEL lead to DMD (ester vs. ketone) with improved withdrawing ability (counterproductive saturation of the carbonyls by alkoxy groups in MEL).
- Chalcogenide O→S replacement as in DBB vs. DBTB significantly affects properties of both acceptors. The latter proved much stronger.
- O→N replacements as in CAA vs. MDN or MEL vs. DBB enhances the withdrawing power and, therefore, MDN and DBB are stronger acceptors than CAA and MEL, respectively.
- When comparing 1,3-diketones DMD and IND, the latter showed much stronger withdrawing ability as a result of the fused benzene ring allowing enlarged conjugation.

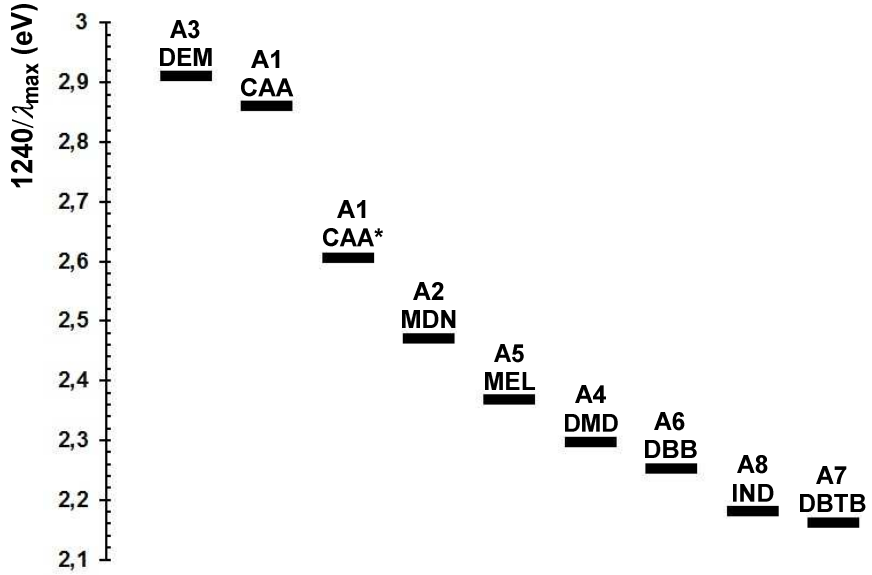

Figure 8. *Comparison of averaged optical gaps ($1240/\lambda_{max}$) for the particular series of MA-derived withdrawing units. * Acetic acid was added.*

3.1.5 Quantum chemical calculation

Spatial and electronic properties of all target chromophores **A1**-**A8** were investigated at the DFT level using Gaussian W09 package.[38] The geometries of molecules **A1**–**A8** were optimized by DFT B3LYP/6-311++G(2d,p) method. Energies of the HOMO and LUMO, their differences, ground state dipole moments μ and first hyperpolarizabilities β were also calculated on the DFT B3LYP/6-311++G(2d,p) level. All calculated data are summarized in *Table 2*.

Table 2. *DFT calculated parameters of chromophores **A1–A8**.*

Comp.	E_{HOMO} (eV)[a]	E_{LUMO} (eV)[a]	ΔE^{DFT} (eV)	μ[a] (D)	$\beta \cdot 10^{-30}$ (esu)[a]	Comp.	E_{HOMO} (eV)[a]	E_{LUMO} (eV)[a]	ΔE^{DFT} (eV)	μ[a] (D)	$\beta \cdot 10^{-30}$ (esu)[a]
1a	-5.75	-2.46	3.29	10.9	34	**1c**	-6.40	-3.14	3.26	12.5	47
2a	-5,89	-2.67	3.22	12.8	38	**2c**	-6.69	-3.41	3.28	9.4	43
3a	-5.39	-1.92	3.47	7.1	52	**3c**	-5.73	-2.08	3.65	2.3	53
4a	-5.54	-2.31	3.23	6.8	57	**4c**	-5.86	-2.74	3.12	3.4	92
5a	-5.71	-2.39	3.32	8.3	41	**5c**	-6.17	-2.89	3.28	5.1	67
6a	-5.65	-2.41	3.24	9.2	51	**6c**	-5.99	-2.89	3.10	5.9	86
7a	-5.69	-2.63	3.06	10.9	30	**7c**	-6.05	-3.19	2.86	6.9	370
8a	-5.52	-2.47	3.05	6.9	134	**8c**	-5.76	-2.89	2.87	4.7	295
1b	-5.57	-2.76	2.81	15.4	194	**1d**	-5.99	-3.29	2.70	14.9	659
2b	-5.66	-2.88	2.78	15.1	182	**2d**	-6.39	-3.57	2.82	8.7	304
3b	-5.27	-2.25	3.02	10.4	198	**3d**	-5.74	-2.73	3.01	7.8	288
4b	-5.34	-2.61	2.73	8.6	319	**4d**	-5.60	-3.00	2.60	5.5	3343
5b	-5.48	-2.68	2.80	10.2	233	**5d**	-5.82	-3.13	2.69	7.0	906
6b	-5.44	-2.70	2.74	11.1	299	**6d**	-5.74	-3.12	2.62	9.0	2316
7b	-5.49	-2.88	2.61	13.1	368	**7d**	-5.82	-3.35	2.47	11.3	829
8b	-5.34	-2.69	2.65	8.5	707	**8d**	-5.74	-3.08	2.66	4.0	28222[b]

[a] Calculated at the DFT B3LYP/6-311++G(2d,p) level; [b] Most likely overestimated value (repeated calculations always with the same result).

The calculated energies of the HOMO and LUMO of **A1**–**A8** range from −6.69 to −5.27 and from −3.57 to −1.92 eV, respectively. They are obviously a function of the branching, extension of the π-linker, and type of the attached acceptor moiety. The calculated HOMO-LUMO gaps (ΔE^{DFT}) are generally a bit wider than those obtained by electrochemistry, however the trends within the whole series of molecules are clearly preserved (*Figure 6*). Moreover, the calculated HOMO-LUMO differences correlate tightly with both electrochemical and optical gaps and, therefore, the used DFT method can be considered as a reasonable tool describing electronic properties of **A1**–**A8**. For instance, the narrowest ΔE^{DFT} of 2.47 eV was calculated for chromophore **A7d** with DBTB acceptor moiety, similarly to the electrochemical

outcome. In general, the averaged ΔE^{DFT} values of **A1–A8** decrease in the order of DEM > CAA ≈ MDN ≈ MEL > DMD ≈ DBB > IND > DBTB, which resembles the order deduced from the electrochemical and optical properties.

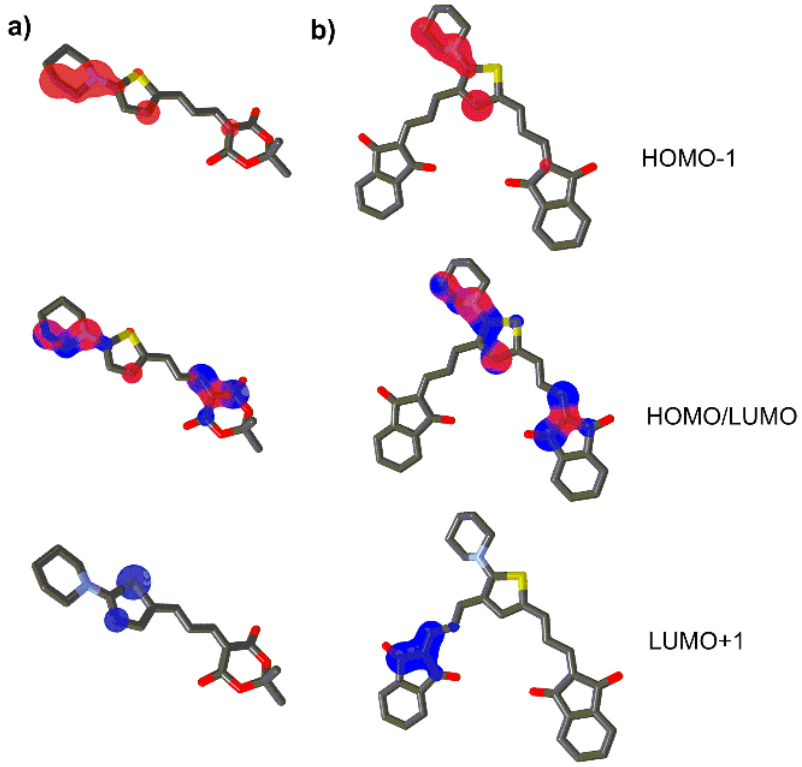

Figure 9. *HOMO/HOMO-1 (**red**) and LUMO/LUMO+1 (**blue**) localizations in **A5b** (a) and **A8d** (b).*

The HOMO and LUMO localizations in representative chromophores **A5b** and **A8d** are shown in *Figure 9*. Molecules in linear series **a** and **b**, e.g. **A5b**, possess the HOMO and the HOMO-1 localized predominantly on the piperidinyl donor and partially in the alternating positions. The LUMO is spread over the MEL acceptor part, adjacent π-linker, and partially also on the piperidinyl residue. The LUMO+1 is localized on the thiophene central part. Branched chromophores in series **c** and **d**, e.g. **A8d**, showed very similar localization of the HOMO and HOMO-1, whereas the LUMO is spread mostly over the IND acceptor appended on the remote branch. The second branch closer to the piperidinyl donor is occupied by the LUMO+1. This distribution of the LUMO orbitals is a common feature of branched push-pull molecules.[25] Surprisingly, chromophores **A7a–d** have the HOMO localized on the sulphur and oxygen atoms of the DBTB acceptor.

The calculated ground state dipole moments range from 2.3 to 15.4 D (*Table 2*). In general, the highest values were calculated for chromophores with CAA (**A1a–d**), MDN (**A2a–d**), and DBTB (**A7a–d**) acceptors (9–15 D). On the contrary, chromophores with 1,3-diketo acceptors such as DMD (**A4a–d**) and IND (**A8a–d**) showed significantly diminished μ values

(2–8 D). Extension of the π-linker generally increased the dipole moment, while branching has rather opposite effect.

Polarizabilities of the chromophores **A1–A8** have also been evaluated by calculating the first hyperpolarizabilities β (*Table 2*). Excluding **A8d** as an outlier, the calculated β values range from $30 \cdot 10^{-30}$ to $3343 \cdot 10^{-30}$ esu. Compared to linear chromophores **A1a–A8a** ($\beta = 30–134 \cdot 10^{-30}$ esu), extension of the π-linker as in **A1b–A8b** resulted in significant improvement of the first hyperpolarizability β up to $182–707 \cdot 10^{-30}$ esu. Similar and even pronounced trend can be seen when comparing series **c** and **d**. Branched chromophores in series **c** and **d** possess up to one order of magnitude higher β values than the corresponding linear analogues in series **a** and **b**. From the MA-derived acceptor moieties, the DBTB and IND impart the strongest ICT into the molecule, which also reflects their generally highest calculated NLO coefficients in series **a–c**. However, in the branched and most extended series **d**, the highest β values were calculated for **A4d**, **A6d**, (and **A8d**) bearing 1,3-diketo (DMD and IND) or DBB acceptors. Hence, indan-1,3-dione and (thio)barbituric acids seems to be the most powerful acceptors from the whole series of push-pull molecules.

3.1.6 Conclusion

In order to study withdrawing ability of six malonic acid derivatives and two its analogues, new model push-pull chromophores have been designed and synthesized. First, a straightforward reaction path towards four PIT aldehydes has been developed. These aldehydes underwent smooth Knoevenagel condensation with eight different MA-derivatives to afford 32 mostly new push-pull molecules **A1–A8** in four series **a–d**. These chromophores have systematically varied peripheral acceptor moiety, structural arrangement, and length of the π-linker. Thorough structure-property relationships have been elucidated considering both experimental (thermal, electrochemical, and optical) and calculated data.

Molecular structures of all PIT aldehydes **A9a–d** as well as five target chromophores **A2c**, **A4a**, **A5b**, and **A8a–b** were confirmed by X-ray analysis, which revealed considerably planar structures, high quinoid character of the central thiophene ring, and extensive π–π stacking in the solid state. DSC analysis showed that π-linker extension decreased thermal robustness, branching mostly caused direct decomposition without melting, and variation of the peripheral withdrawing moiety affected thermal property of **A1–A8** according to its nature. Hence, the highest thermal robustness has been observed for MDN-terminated molecules as well as for CAA-, DEM-, and IND-derivatives.

The electrochemical and UV/Vis absorption optical measurements revealed the same trends and structural features influencing the fundamental properties of target chromophores **A1**–**A8**. Namely, the π-linker extension and gradual chromophore branching reduces both electrochemical and optical gaps. However, the HOMO/LUMO levels and resulting gaps are predominantly dictated by the composition, electronic, and spatial nature of the used acceptor. A replacement of the particular atoms (O→C, O→N, and O→S) within the acceptor unit significantly improves its electron withdrawing ability. Cyclic acceptors proved to be stronger than linear analogues. Extended π-conjugation (e.g. IND) further enhances withdrawing behavior. The aforementioned conclusion are further fully supported by the performed DFT calculations. The calculated data correlates tightly with the electrochemical and optical properties.

Hence, based on the experimental as well as calculated properties, the particular MA-derived acceptors can be ordered as follows:

DEM ≤ CAA < MDN < MEL < DMD ≤ DBB < IND ≤ DBTB.

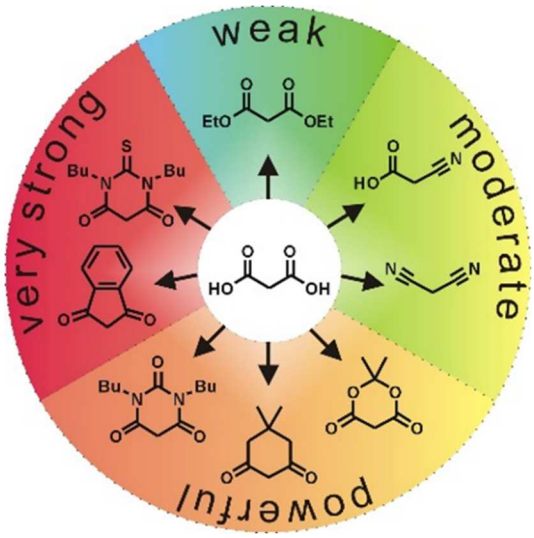

Figure 10. *Visualization of the electron-withdrawing ability of the particular MA-derivatives and its 1,3-diketo analogues.*

In general, the MA-derived acceptors can be classified in four subgroups (*Figure 10*):

- weak (DEM),
- moderate (CAA, MDN),
- powerful (MEL, DMD, DBB),
- and very strong (IND, DBTB).

The main goal of this work was to investigate and critically compare the withdrawing ability of the most used MA-derived acceptors. Therefore, a wide range of target

MA-chromophores has been synthesized based on the PIT donor, which allowed proper evaluation of averaged experimental and theoretical results. I believe that the deduced outcomes may serve as a useful guide to conveniently select a proper MA-derivative for the given D-π-A system with desired optoelectronic behavior.

3.2 Multipodal arrangement of push-pull chromophores

3.2.1 Thermal properties

Thermal behavior of compounds **B1**–**B24** was studied by differential scanning calorimetry (DSC). *Figure 11* shows thermograms of three representative compounds **B7**, **B12**, and **B24** while *Table 3* lists all the measured melting points (T_m) and temperatures of thermal decompositions (T_d). The measured melting points of **B1**–**B24** range from 108 to 226 °C and the temperature of decomposition was estimated within the range of 115–396 °C.

Compound **1** provided very sharp peak of melting/crystallization at 182/147 °C and subsequent evaporation accompanied by the partial decomposition at 332 °C. Compound **B9** exhibited a similar behavior but a complete evaporation at 434 °C with partial decomposition at 392 °C was observed. For chromophore **B2**, the sharp peaks of melting (163 °C), crystallization (148 °C), and decomposition (258 °C) were preceded by moisture/solvent desorption at 100–120 °C. Compounds **B3**, **B8**, **B11** and **B12** showed very gradual decomposition within the range of 70 °C followed by their melting. For **B4**, **B7**, **B15**, and **B19**, the melting process was terminated by an immediate rapid decomposition. The endothermic glass transition about 220 °C and a typical exothermic decomposition of compounds **B6** and **B14** was observed, however their decomposition was also accompanied by an endothermic curving induced probably by their intensive evaporation. For chromophores **B13** and **B14**, a typical monotropic solid-solid transition of metastable crystals was observed at 195 and 120 °C. The relatively weak and broad endothermic peaks in the range of 55–80 and 105–125 °C were recorded for **B16**, **B20**, **B22**, **B23**, and **B18**, respectively. These extended chromophores proved difficult to crystallize and rather represent solidified glassy materials. Hence, the wide peaks most likely represent a glass or solid-solid transitions. On the contrary, compound **B24** showed a very sharp peak of decomposition at 174 °C.

In summary, we can deduce the following outcomes from the DSC measurements:

- Chromophore branching reduces its capability to crystallize (especially for those bearing DBB acceptor unit with long aliphatic butyl chains).

- Some of the quadropolar and most tripodal chromophores showed glass or solid-solid transitions followed by decomposition without melting.
- Compared to DBB derivatives, MDN-terminated molecules showed higher melting points and temperatures of decomposition.
- A very significant reduction of the decomposition temperature of about 100–200 °C was encountered for derivatives with an additional acetylenic spacer (decomposition occurred either immediately or shortly after the melting).
- The chromophores without triple bond(s) are stable even in a liquid state.

Hence, the highest melting point and temperature of decomposition were measured for linear **B9**, quadrupolar **B17** and tripodal **B21** bearing MDN-acceptor moiety, π-linker without triple bonds and TPA central unit.

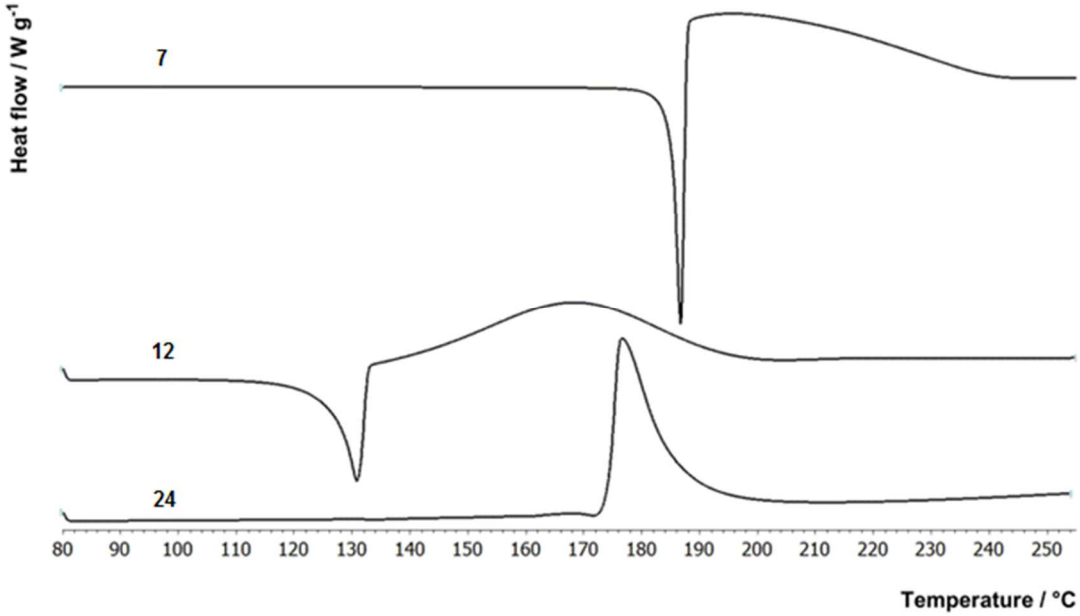

Figure 11. *Representative DSC curves of compounds **B7**, **B12**, and **B24** determined with a scanning rate of 3 °C/min under inert atmosphere of N_2.*

3.2.2 Electrochemistry

Electrochemical measurements of chromophores **B1–B24** were carried out in DMF containing 0.1 M Bu_4NPF_6 in a three electrode cell by cyclic voltammetry (CV), rotating disk voltammetry (RDV), and polarography. The working electrode was platinum disk (2 mm in diameter) for CV and RDV experiments. Other measurement conditions were the same as for the molecules **A1–A8**. The acquired data are summarized in *Table 3*.

The half-wave potentials of the first oxidation and reduction ($E_{1/2(ox1)}$ and $E_{1/2(red1)}$) were found within the range of 0.98 to 1.40 and −1.29 to −0.75 V, respectively. The first oxidation and reduction are typical one-electron processes, followed by subsequent oxidations

and reductions, and are obviously a function of the used acceptor and donor, chromophore arrangements as well as nature of the π-linker. Whereas the first oxidation takes place predominantly on the amino donor, the first reduction is mostly situated on the MDN or DBB acceptors and the adjacent π-linker. The measured half-wave potentials were further recalculated to the energies of the HOMO and the LUMO (*Table 3*).[36] From the measured electrochemical data of **B1**–**B24**, we can draw the following conclusions and structure-property relationships:

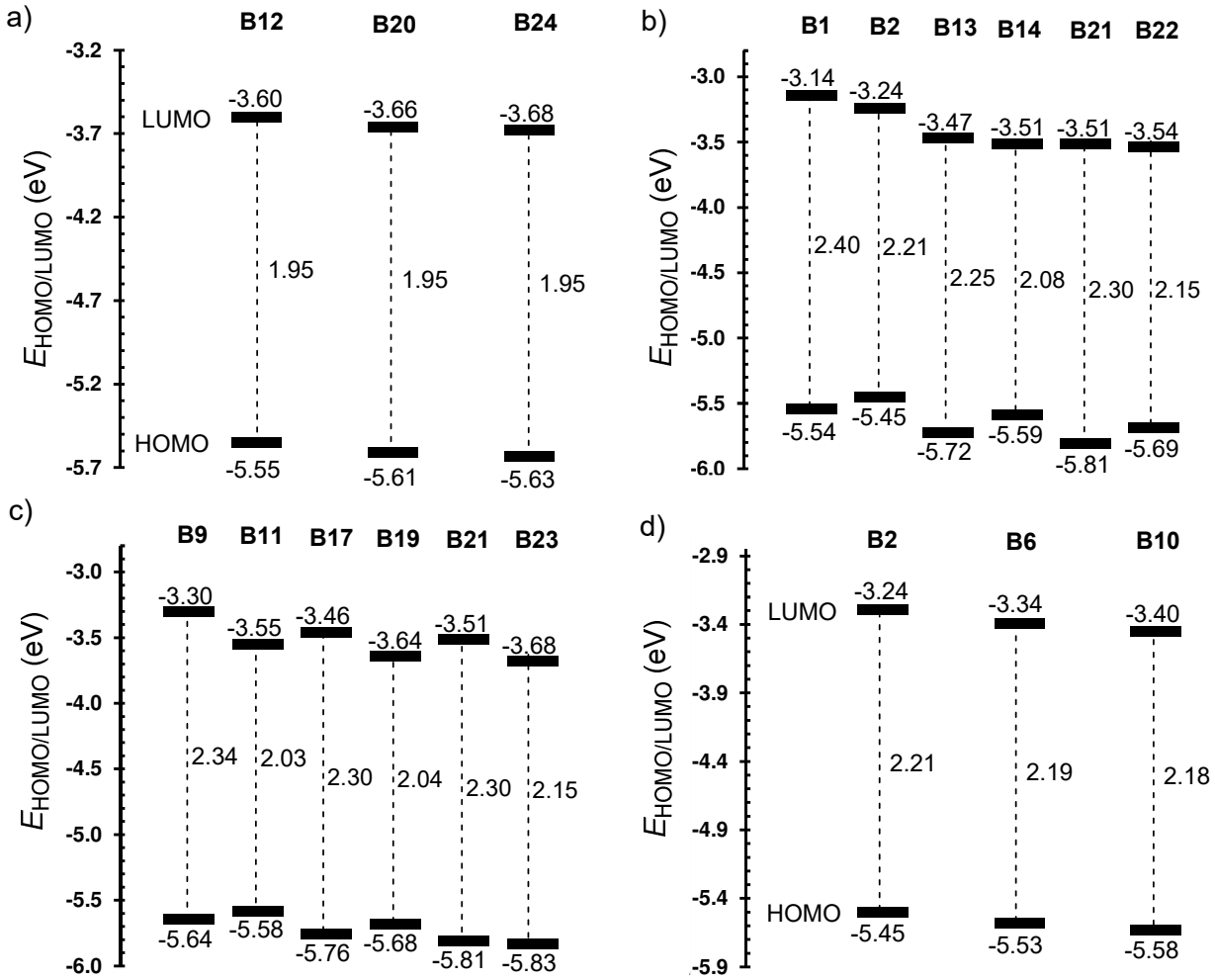

Figure 12. *Energy level diagrams illustrating effect of branching/multipodality (a), impact of the acceptor (b), extension of the π-system (c), and auxiliary N-substituent (d).*

- When going from linear to quadrupolar and tripodal chromophores, the first oxidation/reduction potentials shift steadily to more positive values. In general, chromophore branching/multipodality (number of the acceptors attached to the central amino donor) does not affect the absolute values of the HOMO-LUMO gap (e.g. ΔE of 1.95 eV for **B12**, **B20**, and **B24**, *Figure 12a*). The branching shifts the HOMO and LUMO levels more deeply instead.

- Replacement of the MDN by DBB acceptor is accompanied by a decrease/increase of the first oxidation/reduction potentials, respectively. Energy level diagram in *Figure 12b* illustrates impact of both acceptors on pairs of chromophores **B1**/**B2** (linear), **B13**/**B14** (quadrupolar), and **B21**/**B22** (tripodal). Whereas the acceptor replacement affects both HOMO and LUMO levels for linear molecules **B1** and **B2** similarly, its impact on the LUMO of branched molecules is diminished. Hence, the LUMO levels of **B13**/**B14** and **B21**/**B22** are almost identical and the principal changes are seen on the HOMO.
- Extension of the π-linker by an additional electronegative acetylenic spacer is accompanied by a similar reduction of the ΔE as seen for the MDN→DBB replacement. This is demonstrated in *Figure 12c* for **B9**/**B11**, **B17**/**B19**, and **B21**/**B23**. However, in contrast to the aforementioned variation of the acceptor, the HOMO becomes steady with increased number of branches and the HOMO-LUMO gap is mostly dictated by the LUMO.
- Auxiliary substituents attached to the amino donor (Me or Ph) affect the electrochemical behavior of **B1**–**B24** in a very similar way as branching. Energy level diagram for chromophores **B2**, **B6**, and **B10** shown in *Figure 12d* depicts their almost identical gap (ΔE ~ 2.2 eV) and gradually lowered HOMO/LUMO levels.

The aforementioned observations imply that the electrochemical behavior of **B1**–**B24** can be systematically tuned both in terms of its absolute value (ΔE) as well as frontiers of the gap (E_{HOMO} and E_{LUMO}).

3.2.3 One photon absorption

All target chromophores **B1**–**B24** are intensely colored solids with a color ranging from yellow to purple. Hence, linear optical properties were examined by UV-Vis spectroscopy. Some chromophores showed very weak fluorescence, most of them none (especially those with DBB acceptor), and, therefore emission properties of **B1**–**B24** were not investigated. The longest-wavelength absorption maxima λ_{max} as well as molar absorption coefficients ε_{max} are summarized in *Table 3*. The longest-wavelength absorption maxima λ_{max} range from 432 to 517 nm with the molar absorption coefficients ε_{max} of $25 \cdot 10^3$–$90 \cdot 10^3$ $M^{-1}cm^{-1}$. In a similar way as above, fundamental structure-property relationships can be elucidated:

- Linear chromophores **B1**–**B12** exhibited always one CT-band, which position range from 432 to 503 nm.

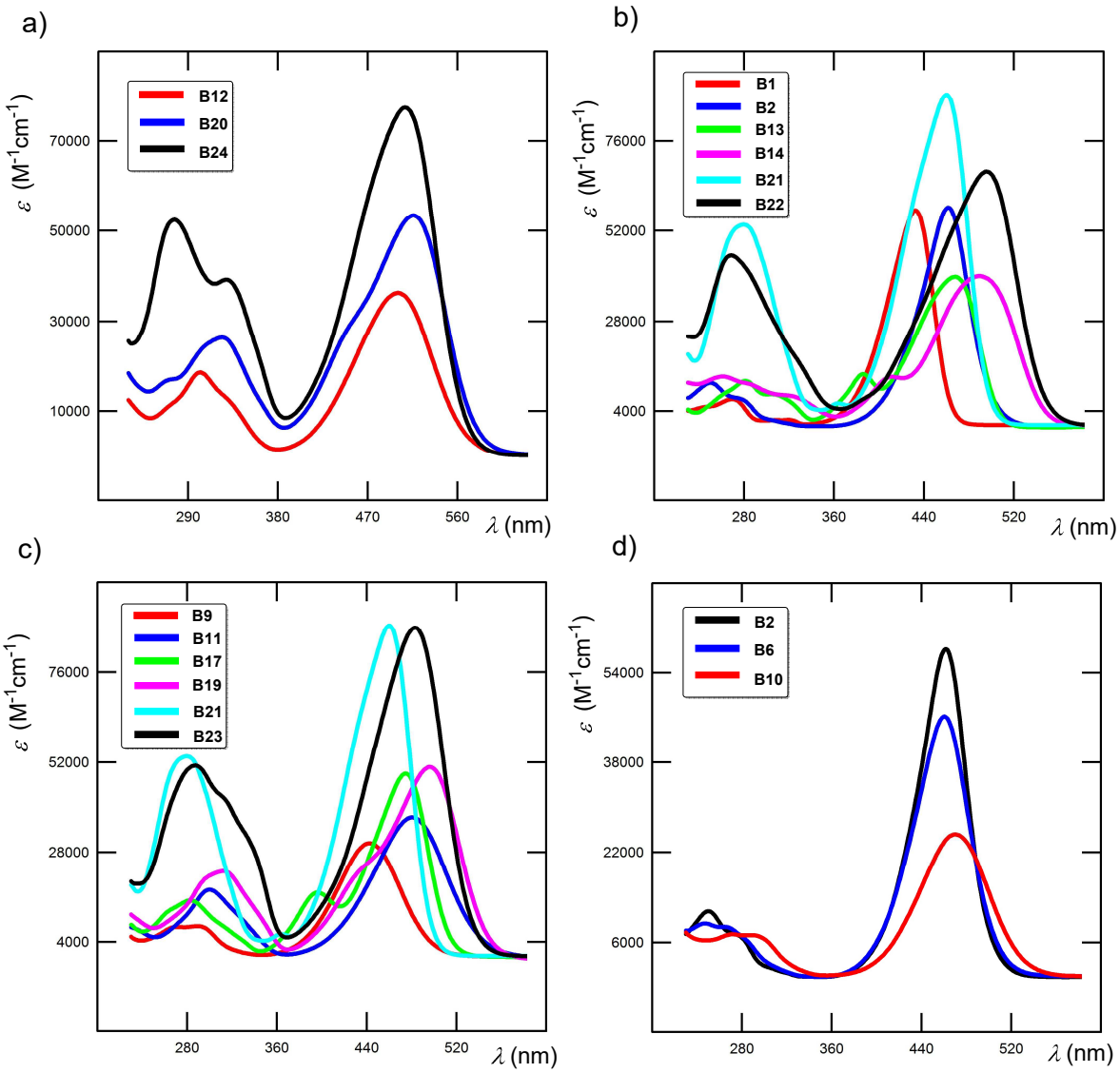

Figure 13. *UV-Vis spectra ($2 \cdot 10^{-5}$ M sol. in CH_2Cl_2) of selected chromophores illustrating effect of branching/multipodality (a), impact of the acceptor (b), extension of the π-system (c), and auxiliary N-substituent (d).*

- The absorption spectra of quadrupolar chromophores **B13–B20** showed two peaks. Beside the main peak (468–517 nm), a shoulder located on the high-energy side of the main peak (~400 nm) is observed. This splitting results from the coupling between branches and can be explained by the Frenkel exciton model.[37]
- Accordingly, the absorption spectra of tripodal molecules should exhibit three bands (excited states). However, the two states are degenerated and lie at the low-energy side of the corresponding linear chromophore's excited state, while the third one is located on the high-energy side and is predicted to have zero oscillator strength. As a result, tripodal molecules **B21–B24** showed one intense CT-band with the position ranging from 460 to 509 nm.

Table 3. *Summary of thermal, electrochemical, linear and nonlinear optical properties of chromophores **B1–B24**.*

Comp.	T_m (°C)[a]	T_d (°C)[b]	$E_{1/2(ox1)}$ (V)[c]	$E_{1/2(red1)}$ (V)[c]	ΔE (eV)[c]	E_{HOMO} (eV)[e]	E_{LUMO} (eV)[e]	λ_{max}^{A} (nm/eV)[f]	$\varepsilon_{max}^{A} \cdot 10^3$ ($M^{-1} \cdot cm^{-1}$)[f]	$PO \cdot 10^{-14}$ (m^2/N)[g]
B1	182	332	1.11	–1.29	2.40	–5.54	–3.14	433/2.86	58.5	3.01
B2	163	258	1.02	–1.19	2.21	–5.45	–3.24	461/2.69	59.2	3.18
B3	131	139	1.03	–0.93	1.96	–5.46	–3.50	479/2.59	48.6	3.30
B4	143	149	0.98	–0.90	1.88	–5.41	–3.53	503/2.47	37.7	3.93
B5	115	346	1.17	–1.22	2.39	–5.60	–3.21	432/2.87	48.3	2.81
B6	142	286	1.10	–1.09	2.19	–5.53	–3.34	460/2.70	46.8	3.06
B7	185	187	1.13	–0.91	2.04	–5.56	–3.52	474/2.62	45.1	3.16
B8	119	127	1.06	–0.86	1.92	–5.49	–3.57	497/2.49	31.6	3.90
B9	139	392	1.21	–1.13	2.34	–5.64	–3.30	442/2.81	30.6	3.15
B10	108	357	1.15	–1.03	2.18	–5.58	–3.40	468/2.65	25.4	2.86
B11	178	184	1.15	–0.88	2.03	–5.58	–3.55	481/2.58	37.6	3.01
B12	126	138	1.12	–0.83	1.95	–5.55	–3.60	501/2.48	36.5	3.12
B13	206	340	1.29	–0.96	2.25	–5.72	–3.47	468/2.65	40.1	3.19
B14	134	277	1.16	–0.92	2.08	–5.59	–3.51	486/2.55	40.3	3.09
B15	182	189	1.33	–0.81	2.14	–5.76	–3.62	488/2.54	46.8	3.15
B16	-	115	1.14	–0.78	1.92	–5.57	–3.65	509/2.44	50.1	3.16
B17	226	396	1.33	–0.97	2.30	–5.76	–3.46	475/2.61	49.7	3.21
B18	-	260	1.20	–0.92	2.12	–5.63	–3.51	503/2.47	51.4	3.32
B19	195	201	1.25	–0.79	2.04	–5.68	–3.64	497/2.49	51.1	3.16
B20	-	153	1.18	–0.77	1.95	–5.61	–3.66	517/2.40	53.6	4.13
B21	218	373	1.38[d]	–0.92[d]	2.30	–5.81	–3.51	460/2.70	89.7	3.20
B22	-	281	1.26	–0.89	2.15	–5.69	–3.54	496/2.50	68.3	3.14
B23	-	182	1.40[d]	–0.75[d]	2.15	–5.83	–3.68	483/2.57	88.6	3.12
B24	-	174	1.20	–0.75	1.95	–5.63	–3.68	509/2.44	77.9	3.35

[a]T_m = melting point (the point of intersection of a baseline before the thermal effect with a tangent). [b]T_d = thermal decomposition (pyrolysis in N_2 atmosphere). [c]$E_{1/2(ox1)}$ and $E_{1/2(red1)}$ are half-wave potentials of the first oxidation and reduction, respectively; all potentials are given vs. SCE; $\Delta E = E_{1/2(ox1)} - E_{1/2(red1)}$; scan rate 100 mV.$s^{-1}$ for CV. [d]Only peak potentials, RDV records can´t be evaluated due to inhibition of the electrode. [e] $-E_{HOMO/LUMO} = E_{1/2(ox1/red1)} + 4.429$. [f]Measured in CH_2Cl_2. [g]Maximally achieved photoinduced piezooptic coefficients at cw He-Ne laser probing wavelength 1150 nm. The data are presented with corrections on scattering background.

- Hence, when going from linear to quadrupolar and tripodal chromophores, the CT-bands can be either single or structured with increased molar absorption coefficient (e.g. from **B10** to **B21** is $\Delta\varepsilon_{max}$ equal to 64350 $M^{-1}cm^{-1}$). The position of the longest wavelength absorption maxima is affected only negligibly (*Figure 13a*).
- A clear trend of bathochromically shifted CT-band of DBB over MDN substituted chromophores, has been encountered across all structural arrangements. A red-shift of about 20–40 nm can be seen in the pairs of molecules differing only in the acceptor unit (*Figure 13b*).

- Compared to MDN-substituted chromophores, attaching stronger electron withdrawing DBB unit to linear and tripodal chromophores reduces their molar absorption coefficients. This is in contradiction to quadrupolar molecules (*Figure 13b*).
- Extension and planarization of the chromophore π-backbone via an additional triple bond enhances the ICT which is reflected by a red shift of the λ_{max} by about 20–40 nm for the given pair of molecules (*Figure 13c*).
- Replacement of the auxiliary substituents attached on the amino donor has only diminished effect on λ_{max}, especially for the linear molecules **B1**–**B12** (*Figure 13d*).

In general, the measured optical properties confirm the conclusions made from electrochemical measurements.

3.2.4 Nonlinear optical (NLO) properties – piezooptical effect

Push-pull molecules can generally be designed towards second- and third-order NLO. Third-order NLO is described by third rank polar tensors, which may occur both in centrosymmetrical and non-centrosymmetrical media. Among several known nonlinear optical effects, a particular attention is currently devoted to third harmonic generation (THG), two and multi photon absorption (2PA and MPA), electro-optic Kerr effect and piezooptical effects *PO*.[39] Generally, the piezooptical (elasto-optical) effect is described by fourth rank polar tensors. The effect is caused by the changes of birefringence under applied mechanical stress. Contrary to similar third-order nonlinear optical effects (2PA or THG), the piezooptics depends both on electronic and phonon (vibration) contributions. Simultaneously, the ground state dipole moments and spectral positions of the first UV absorption maxima play principal role. Hence, its relation to the microscopic third order optical nonlinearities is not trivial.

The particular chromophores **B1**–**B24** were embedded into the PVA polymer matrices and were grown in a form of films with thickness about 1–3 μm by spin coated technique. [40] The optimal concentration with respect to piezooptical response of the chromophore (giving maximal piezooptical response) was varied within the 10–15 mol. %. The susceptibility of the method was enhanced during use of additional photo-treatment.[41] For this reason it was performed additional photo-polarization of the samples using three types of photo-induced treatments as presented in *Figure 14*, which depicts principal experimental changes of the photo-induced piezooptics for the composites measured by a standard method.[42] Maximally achieved photo-induced piezooptic coefficients *PO* are listed in *Table 3*. From these data the following structure-property relationships can be deduced:

- Within the series of linear molecules **B1**–**B12**, the *PO* generally increase from **B1**–**B4**, **B5**–**B8**, and **B9**–**B12** as a result of the extension of the π-system and replacement of MDN by DBB acceptors.
- A comparison of linear chromophores **B4**, **B8**, and **B12** with the highest *PO*s reveals rather detrimental effect of the chromophore extension via auxiliary *N*-substituents. The *PO* decrease in the following order of substituents: diMe > PhMe > diPh.
- A monotonous increase of the *PO*s can be seen when going through the series of quadrupolar chromophores **B13**–**B20**. Chromophore **B19**, which showed exceptionally high calculated ground state dipole moment (*chapter 3.2.5*), is an exception.
- Chromophore **B20** with two DBB acceptors and extended π-system showed the highest $PO = 4.13 \cdot 10^{-14}$ m^2/N.
- A very similar trend can also be observed within tripodal molecules **B21**–**B24** with the largest *PO* measured for **B24**.

Similarly to electrochemical and optical properties, the piezooptical effect in **B1**–**B24** is affected mostly by the chromophore arrangement, electron withdrawing nature of the appended acceptor unit, extension of the π-linker, and type of the auxiliary *N*-substituent. Hence, the largest *PO*s within the particular series were measured for chromophores **B4**/**B8**/**B12**, **B20**, and **B24**.

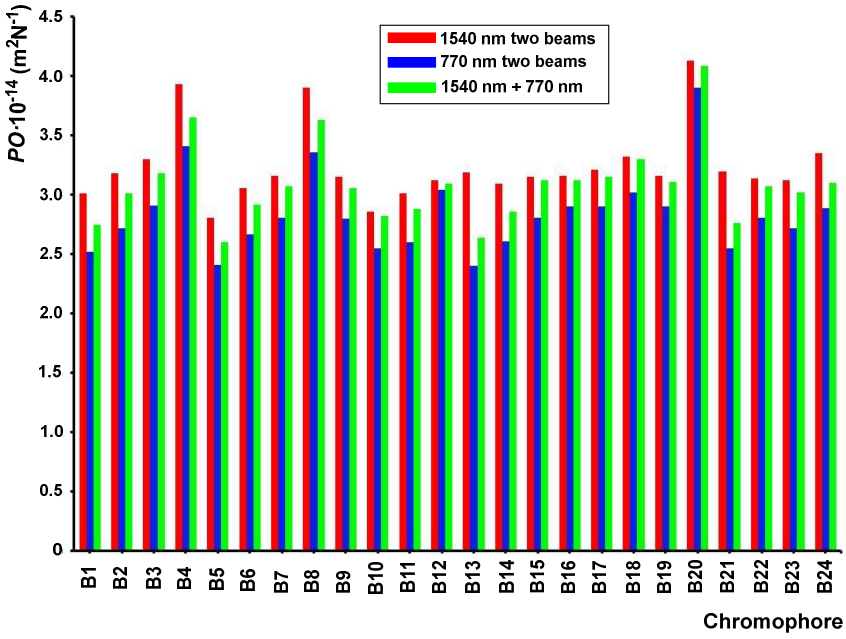

Figure 14. *Dependence of the effective off-diagonal piezooptic coefficient PO at wavelength 1150 nm of cw He-Ne laser for different samples at three different regime of treatment: 1540 nm two coherent nanosecond laser beams; 770 nm two coherent nanosecond pulsed 770 nm laser beam; 1540 nm + 770 nm bicolor coherent laser beam treatment.*

Table 4. *DFT calculated properties of chromophores **B1–B24**.*

Com.	E_{HOMO} (eV)[a]	E_{LUMO} (eV)[a]	ΔE_{DFT} (eV)[a]	μ (D)[a]	$\beta \cdot 10^{-29}$ (esu)[b]	$\gamma \cdot 10^{-42}$ (esu)[b]	Com.	E_{HOMO} (eV)[a]	E_{LUMO} (eV)[a]	ΔE_{DFT} (eV)[a]	μ (D)[a]	$\beta \cdot 10^{-29}$ (esu)[b]	$\gamma \cdot 10^{-42}$ (esu)[b]
B1	–6.10	–2.65	3.45	11.53	3.28	55.4	**B13**	–6.53	–3.56	2.97	3.39	2.27	222.0
B2	–5.82	–2.42	3.40	7.62	3.06	69.7	**B14**	–6.02	–3.10	2.92	4.32	2.08	183.5
B3	–5.97	–2.99	2.98	12.52	5.04	149.2	**B15**	–6.32	–3.65	2.67	9.75	3.92	597.0
B4	–5.71	–2.74	2.97	8.78	4.72	168.8	**B16**	–5.96	–3.32	2.64	5.55	3.81	617.5
B5	–6.09	–2.67	3.42	11.66	3.41	104.9	**B17**	–6.41	–3.48	2.93	9.30	2.93	287.7
B6	–5.82	–2.46	3.36	7.46	2.70	121.2	**B18**	–6.00	–3.13	2.87	4.04	2.20	293.1
B7	–5.96	–3.00	2.96	12.57	5.16	196.5	**B19**	–6.22	–3.58	2.64	14.05	4.92	571.6
B8	–5.72	–2.77	2.95	8.39	4.90	219.4	**B20**	–5.90	–3.28	2.62	4.45	5.03	743.5
B9	–5.96	–2.83	3.13	10.66	4.80	179.2	**B21**	–6.75	–3.78	2.97	5.84	0.27	363.5
B10	–5.72	–2.62	3.10	6.16	2.44	162.4	**B22**	–6.16	–3.28	2.88	0.65	0.43	411.0
B11	–5.87	–3.14	2.73	11.33	6.20	302.0	**B23**	–6.49	–3.88	2.61	7.75	0.29	861.9
B12	–5.65	–2.90	2.75	6.95	5.59	330.1	**B24**	–6.05	–3.42	2.63	1.12	0.44	1033.6

[a]Calculated at the DFT B3LYP/6-311++G(2d,p) level. [b]Calculated by MOPAC2012.

3.2.5 Quantum chemical calculations

Spatial and electronic properties of linear, quadrupolar and tripodal chromophores **B1–B24** were investigated by DFT calculations using Gaussian W09 package.[38] Initial geometries were estimated by PM3 method implemented in ArgusLab[43] and these were subsequently optimized by DFT B3LYP/6-311++G(2d,p) method. Energies of the HOMO and the LUMO, their differences, and ground state dipole moments were also calculated with the DFT B3LYP/6-311++G(2d,p). A replacement of the butyl substituents in DBB moiety (**B16**, **B18**, **B20**, **B22**, and **B24**) by methyl groups has been made to accelerate the DFT calculations. This substitution has almost zero influence on the electron density distribution along the molecule. The first and second hyperpolarizabilities β and γ were deduced from the optimized geometries by employing PM7 method implemented in MOPAC2012.[44] All calculated data are summarized in *Table 4*.

The calculated energies of the HOMO/LUMO of **B1–B24** range from –6.75/–5.65 to –3.88/–2.42 eV. The calculated ΔE_{DFT} range from 3.45 to 2.61 eV. Both energies as well as HOMO-LUMO gaps correlate well with the experimental HOMO/LUMO values obtained from the electrochemical and optical measurements. Similar trends as deduced from the electrochemistry and electronic absorption spectra can also be seen from the calculated data. Namely, ΔE_{DFT} depends primarily on the branching, character of the acceptor, π-linker extension/planarity as well as auxiliary *N*-substituent. Whereas extension of the π-linker

by an additional acetylenic spacer affects the gaps very significantly (e.g. **B1** vs. **B3** or **B10** vs. **B12**, *Table 4*), replacement of the peripheral acceptor MDN→DBB has diminished effect (e.g. **B1** vs. **B2** or **B11** vs. **B12**). In contrast to electrochemical measurements, the calculated gaps steadily decrease when going from linear to quadrupolar and tripodal systems with the largest one being calculated for **B1** and the lowest one for **B23**/**B24**.

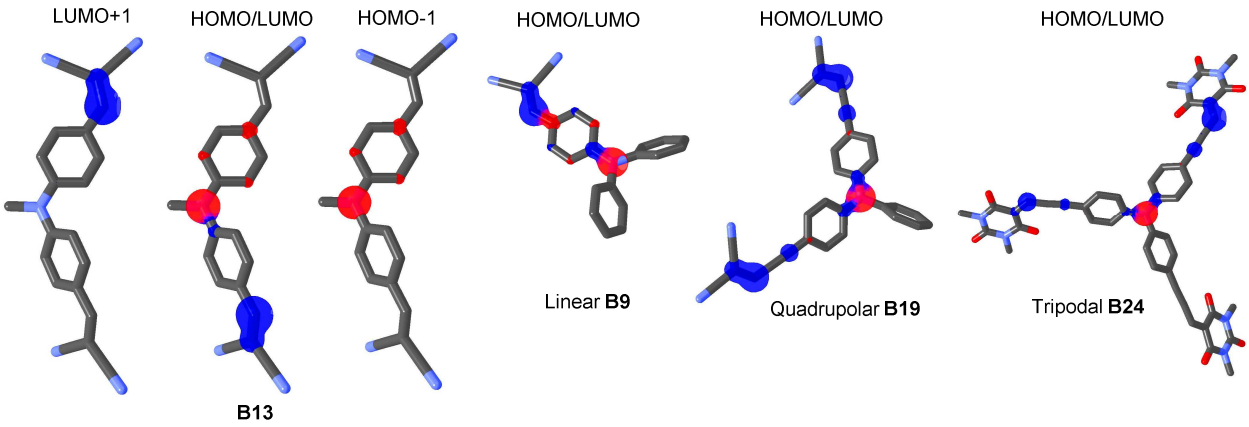

Figure 15. *HOMO/HOMO−1 and LUMO/LUMO+1 localizations in **B13** and HOMO/LUMO mix in **B9**, **B19** and **B24**.*

The HOMO and LUMO localizations in representative chromophores **B9**, **B13**, **B19** and **B24** are shown in *Figure 15*, which shows clear charge separation and thus confirm ICT character of chromophores **B1**–**B24**. As a general trend, the HOMO as well the HOMO−1 is localized on the amino donor and the adjacent alternating positions of the phenyl ring(s), whereas the LUMO is spread over the peripheral MDN or DBB acceptor(s) and the adjacent π-linker. This holds true especially for linear chromophores **B1**–**B12**. In quadrupolar molecules **B13**–**B16** are the HOMO/HOMO−1 localized on the central amino donor and adjacent phenyl ring of the first branch, whereas the LUMO is spread over the second branch. The LUMO+1 occupy the first branch. On the other hand, in quadrupolar molecules **B17**–**B20** with TPA donor is the LUMO situated on both branches. Tripodal chromophores **B21**–**B24** possess the LUMO spread over one or two particular branch(es), while the third branch is occupied by the LUMO+1. The HOMO as well the HOMO−1 remained on the central amino acceptor. This is a common feature of tripodal molecules based on triphenylamine.[45]

The calculated ground state dipole moments (*Table 4*) range from 6 to 12.5 D for linear molecules **B1**–**B12** and are generally less for quadrupolar chromophores **B13**–**B20** (except **B19**). Tripodal molecules **B22** and **B24** featuring DBB acceptors showed very low ground state dipole moments, whereas much larger values were obtained for tripodal molecules **B21** and **B23** with MDN acceptors. Except **B22**, all tripodal molecules possess *C*3 group of symmetry.

Molecular second- and third-order optical nonlinearities β and γ were calculated as well (*Table 4*). As can be seen, both polarizabilities showed reversal trends. Whereas β coefficients generally decrease with the chromophore branching/symmetrization, the values of γ steadily increase when going from **B1**–**B24**. Moreover, the calculated third-order polarizabilities mimic the trends seen for experimentally obtained POs. Namely, the third-order NLO response significantly increases with chromophore branching, extension of the π-system and less by the acceptor replacement and type of the auxiliary *N*-substituent.

3.2.6 Conclusion

A series of twenty four model push-pull chromophores (16 new) has been designed and synthesized employing iodination, Sonogashira cross-coupling reaction, and final Knoevenagel condensation. These chromophores systematically vary in spatial arrangement (linear **B1**–**B12**, quadrupolar **B13**–**B20**, and tripodal **B21**–**B24**), withdrawing nature of the peripheral acceptor (MDN vs. DBB), extension of π-system, and type and number of methyl/phenyl groups attached to the amino donor. A thorough elucidation of the structure-property relationships has been performed based on thermal, electrochemical, UV-Vis absorption, and piezooptical data further supported by DFT calculations.

Structural features such as branching, MDN→DBB replacement, and insertion of acetylenic units have detrimental effect on thermal stability of **B1**–**B24**. The branching does not affect the absolute values of the electrochemical HOMO-LUMO gaps but rather shifts both HOMO/LUMO levels. A similar effect has been observed for the *N*-substituent, while type of the acceptor and π-system extension reduced the gap significantly. Multipodal arrangement of CT-chromophores also affects shape, size, and position of the absorption maxima. Whereas linear and tripodal molecules showed single CT-bands, quadrupolar chromophores feature two particularly developed bands. A significant red shift has been observed when replacing MDN by DBB acceptors and extending/planarizing the π-system. Type of the auxiliary *N*-substituent influenced absorption optical properties only negligibly. Nonlinear optical properties of **B1**–**B24** were investigated by photo-induced piezooptics. In the descending order, the measured *PO* coefficients were affected by the acceptor, π-system length, branching, and *N*-substituents. Performed DFT calculation further confirmed the experimental conclusion.

The main goal of this work was to shed some light on basic structural features affecting fundamental properties of push-pull chromophores having various arrangements. I believe that the aforementioned findings may serve as a general guide for modulating properties of CT-chromophores.

4. REFERENCES

1. a) S. R. Forrest, M. E. Thompson, *Chem. Rev.* **2007**, *107*, 923; b) R. D. Miller, E. A. Chandross, *Chem. Rev.* **2010**, *110*, 1; c) G. S. He, L.-S. Tan, Q. Zheng, P. N. Prasad, *Chem. Rev*. **2008**, *108*, 1245; d) Y. Ohmori, *Laser Photonics Rev*. **2010**, *4*, 300.
2. a) J. Kulhánek, F. Bureš, J. Opršal, W. Kuznik, T. Mikysek, A. Růžička, *Asian J. Org. Chem.* **2013**, *2*, 422; b) P. D. Jarowski, Y. Mo, *Chem. Eur. J.* **2014**, *20*, 17214; c) H. Meier, *Angew. Chem. Int. Ed.* **2005**, *44*, 2482; d) J. Y. Lee, K. S. Kim, B. J. Mhin, *J. Chem. Phys.* **2001**, *115*, 9484; e) F. Bureš, O. Pytela, M. Kivala, F. Diederich, *J. Phys. Org. Chem.* **2011**, *24*, 274.
3. F. Bureš, *RSC Adv.* **2014**, *4*, 58826.
4. a) H. S. Nalwa, *Adv. Mater.* **1993**, *5*, 341; b) T. Verbiest, S. Houbrechts, M. Kauranen, K. Clays, A. Persoons, *J. Mater. Chem.* **1997**, *7*, 2175; c) D. F. Eaton, *Science.* **1991**, *253*, 281; d) L. R. Dalton, P. A. Sullivan, D. H. Bale, *Chem. Rev.* **2010**, *110*, 25.
5. a) P. Batail, *Chem. Rev.* **2004**, *104*, 4887; b) S. Allard, M. Forster, B. Souharce, H. Thiem, U. Scherf, *Angew. Chem., Int. Ed.* **2008**, *47*, 4070.
6. W. B. Jensen, *J. Chem. Educ.* **2007**, *84*, 924.
7. H. Strittmatter, S. Hildbrand, P. Pollak, Malonic Acid and Derivatives. *Ullmann's Encyclopedia of Industrial Chemistry.* **2012**, *22*, 157–174.
8. a) P. Pollak, G. Romeder, Malonic Acid and Derivatives. *Kirk-Othmer Encyclopedia of Chemical Technology.* **2000**, 1–22.

9 a) R. Menegatti, Green Chemistry – Aspects for the Knoevenagel Reaction in M. Kidwai, N. K. Mishra *(Eds.), Green Chemistry - Environmentally Benign Approaches.* **2012**, 13–32, InTech, Croatia; b) G. Jones, The Knoevenagel Condensation in S. E. Denmark (Ed.), *Organic Reactions*. **2011**, 204–599, John Wiley & Sons, Germany; c) A. M. Asiri, S. A. Khan, H. M. Basisi, *Int. J. Electrochem. Sci.* **2015**, *10*, 6092.

10. a) K. Hara, T. Sato, R. Katoh, A. Furube, Y. Ohga, A. Shinpo, *J. Phys. Chem. B* **2003**, *107*, 597; b) K. Hara, T. Sato, R. Katoh, A. Furube, T. Yoshihara, M. Murai, M. Kurashige, S. Ito, A. Shinpo, S. Suga, H. Arakawa, *Adv. Funct. Mater.* **2005**, *15*, 246; c) L. Giribabu, M. Chandrasekheram, M. L. Kantham, V. G. Reddy, D. Satyanarayana, O. S. Rao, P. Y. Reddy, *Indian J. Chem., Sect A* **2006**, *45*, 629; d) G. Li, K.-J. Jiang, Y.-F. Li, S.-L. Li, L.-M. Yang, *J. Phys. Chem. C* **2008**, *112*, 11591; e) K. Srinivas, K. Yesudas, K. Bhanuprakash, V. J. Rao, L. Giribabu, *J. Phys. Chem. C* **2009**, *113*, 20117; f) K. V. Gupta, J. Zhang, G. Marotta, M. A. Reddy, S. P. Singh, A. Islam, L. Han,

F. De Angelis, M. Chandrasekharam, M. Pastore, *Dyes Pigments*. **2015**, *113*, 536; g) G. S. Reddy, S. Ramkumar, A. M. Asiri, S. Anandan, *Spectrochim. Acta A* **2015**, *145*, 531; h) Y. Wu, W. Zhu, *Chem. Soc. Rev.* **2013**, *42*, 2039.

11. a) M. Kivala, F. Diederich, *Acc. Chem. Res*. **2009**, *42*, 235; b) F. Bureš, W. B. Schweizer, J. C. May, C. Boudon, J.-P. Gisselbrecht, M. Gross, I. Biaggio, F. Diederich, *Chem. Eur. J*. **2007**, *13*, 5378; c) J. C. May, I. Biaggio, F. Bureš, F. Diederich, *Appl. Phys. Lett.* **2007**, *90*, 251106; d) F. Bureš, O. Pytela, F. Diederich, *J. Phys.Org. Chem.* **2009**, *22*, 155; e) F. Bureš, W. B. Schweizer, C. Boudon, J.-P. Gisselbrecht, M. Gross, F. Diederich, *Eur. J. Org. Chem.* **2008**, *6*, 994; f) Y.-L. Wu, F. Bureš, P. D. Jarowski, W. B. Schweizer, C. Boudon, J.-P. Gisselbrecht, F. Diederich, *Chem. Eur. J.* **2010**, *16*, 9592; g) F. Bureš, O. Pytela, M. Kivala, F. Diederich, *J. Phys. Org. Chem.* **2011**, *24*, 274; h) A. Wojciechowski, M. M. Raposo, M. R. Castro, W. Kuznik, I. Fuks-Janczarek, M. Pokladko-Kowar, F. Bureš, *J. Mater. Sci.: Mater. Electron.* **2014**, *25*, 1745.
12. F. Bureš, *Chem. Listy* **2013**, *107*, 834.
13. a) W. Zou, Y. Liu, Q. Jia, Z. Ge, *Chinese J. Org. Chem.* **2013**, *33*, 1522; b) R. V. Pereira, M. H. Gehlen, *Chem. Phys. Lett.* **2006**, *426*, 311 c) C. Coluccini, A. K. Sharma, M. Caricato, A. Sironi, E. Cariati, S. Righetto, E. Tordin, C. Botta, A. Forni, D. Pasini, *Phys. Chem. Chem. Phys.* **2013**, *15*, 1666; d) H. Mokbel, F. Dumur, S. Telitel, L. Vidal, P. Xiao, D.-L. Versace, M.-A. Tehfe, F. Morlet-Savary, B. Graff, J.-P. Fouassier, D. Gigmes, J. Toufaily, T. Hamieh, J. Lalevée, *Polym. Chem.* **2013**, *4*, 5679; e) M. Caricato, C. Coluccini, D. A. Vander Griend, A. Forni, D. Pasini, *New J. Chem.* **2013**, *37*, 2792; f) R. V. Pereira, M. H. Gehlen, *J. Phys. Chem. A* **2006**, *110*, 7539.
14. a) P. Flores, M. C. Rezende, F. Jara, *Dyes Pigments* **2004**, *62*, 277; b) S. E. Boiadjiev, D. A. Lightner, *Monatsh. Chem.* **2008**, *139*, 503; c) L. A. Crawford, H. McNab, *Collect. Czech. Chem. Commun.* **2009**, *74*, 995; d) **S**. Wang, S.-H. Kim, *Dyes Pigments* **2009**, *80*, 314; e) K. Kowalski, Ł. Szczupak, J. Skiba, O. S. Abdel Rahman, R. F. Winter, R. Czerwieniec, B. Therrien, *Organometallics* **2014**, *33*, 4697.
15. a) Y. Nagao, T. Sakai, K. Kozawa, T. Urano, *Dyes Pigments* **2007**, *73*, 344; b) M. C. Rezende, P. Campodonico, E. Abuin, J. Kossanyi, *Spectrochim. Acta A* **2001**, *57*, 1183; c) S.-H. Kim, Y.-S. Kim, D.-H. Lee, Y.-A Son, *Mol. Cryst. Liq. Cryst.* **2011**, *550*, 240.
16. a) M. A. N. Razvi, A. H. Bakry, S. M. Afzal, S. A Khan, A. M. Asiri, *Mater. Lett.* **2015**, *144*, 131; b) S. M. Lee, W. S. Jahng, J. H. Lee, B. K. Rhee, K. H. Park, *Chem. Phys. Lett.* **2005**, *411*, 496; c) J. Garín, J. Orduna, J. I. Rupérez, R. Alcalá, B. Villacampa, C. Sánchez,

N. Martín, J. L. Segura, M. González, *Tetrahedron Lett.* **1998**, *39*, 3577; d) R. Andreu, J. Garín, J. Orduna, R. Alcalá, B. Villacampa, *Org. Lett.* **2003**, *5*, 3143; e) B. R. Cho, J. T. Je, S. J. Lee, S. H. Lee, H. S. Kim, S. J. Jeon, O.-K. Song, C. H. Wang, *J. Chem. Soc., Perkin Trans. 2* **1996**, *10*, 2141; f) X. Zhou, A.-M. Ren, J.-K. Feng, X.-J. Liu, C.-C. Shu, *Chinese J. Chem.* **2004**, *22*, 38.

17. M. El-Sayed, S. Spange, *J. Phys. Org. Chem.* **2007**, *20*, 264.
18. a) K. Zhou, H. Fu, L. Feng, M. Cui, J. Dai, B. Liu, *Chem. Commun.* **2015**, *51*, 11665; b) H. Lee, M. Y. Berezin, K. Guo, J. Kao, S. Achilefu, *Org. Lett.* **2009**, *11*, 29.
19. a) S. Yagai, *J. Photoch. Photobio. C* **2006**, *7*, 164; b) R. B. K. Siram, K. Tandy, M. Horecha, P. Formanek, M. Stamm, S. Gevorgyan, F. C. Krebs, A. Kiriy, P. Meredith, P. L. Burn, E. B. Namdas, S. Patil, *J. Phys. Chem. C* **2011**, *115*, 14369; c) R. Schmidt, M. Stolte, M. Grüne, F. Würthner, *Macromolecules* **2011**, *44*, 3766.
20. M. Klikar, F. Bureš, O. Pytela, T. Mikysek, Z. Padělková, A. Barsella, K. Dorkenoo, S. Achelle, *New. J. Chem.* **2013**, *37*, 4230.
21. R. Nazir, B. Thorsted, E. Balčiunas, L. Mazur, I. Deperasińska, M. Samoć, J. Brewer, M. Farsari, D. T. Gryko, *J. Mater. Chem. C* **2016**, *4*, 167.
22. a) P. Solanke, F. Bureš, O. Pytela, J. Kulhánek, Z. Padělková, *Synthesis* **2013**, *45*, 3044; b) P. Solanke, F. Bureš, O. Pytela, M. Klikar, T. Mikysek, L. Mager, A. Barsella, Z. Růžičková, *Eur. J. Org. Chem.* **2015**, *24*, 5339.
23. a) F. Bureš, H. Čermáková, J. Kulhánek, M. Ludwig, W. Kuznik, I. V. Kityk, T. Mikysek, A. Růžička, *Eur. J. Org. Chem.* **2012**, 529; b) L. Dokládalová, F. Bureš, W. Kuznik, I. V. Kityk, A. Wojciechowski, T. Mikysek, N. Almonasy, M. Ramaiyan, Z. Padělková, J. Kulhánek, M. Ludwig, *Org. Biomol. Chem.* **2014**, *12*, 5517; c) J. Kulhánek, F. Bureš, T. Mikysek, J. Ludvík, O. Pytela, *Dyes Pigm.* **2011**, *90*, 48; d) J. Kulhánek, F. Bureš, O. Pytela, T. Mikysek, J. Ludvík, *Chem. Asian J.* **2011**, *6*, 1604; e) J. Kulhánek, F. Bureš, O. Pytela, T. Mikysek, J. Ludvík, A. Růžička, *Dyes Pigm.* **2010**, *85*, 57.
24. a) V. D. Gupta, A. B. Tathe, V. S. Padalkar, P. G. Umape, N. Sekar, *Dyes Pigm.* **2013**, *97*, 429; b) T. Michinobu, J. C. May, J. H. Lim, C. Boudon, J.-P. Gisselbrecht, P. Seiler, M. Gross, I. Biaggio, F. Diederich, *Chem. Commun.* **2005**, *6*, 737; c) L. Kong, J. Yang, H. Zhou, S. Li, F. Hao, Q. Zhang, Y. Tu, J. Wu, Z. Xue, Y. Tian, *Sci. China: Chem.* **2013**, *56*, 106; d) X. Tang, W. Liu, J. Wu, Ch.-S. Lee, J. You, P. Wang, *J. Org. Chem.* **2010**, *75*, 7273; e) F. Zhou, J. Shao, Y. Yang, J. Zhao, H. Guo, X. Li, S. Ji, Z. Zhang, *Eur. J. Org. Chem.* **2011**, *25*, 4773; f) X. Li, S.-H. Kim, J. Kun, Y.-A. Son, *Mol. Cryst. Liq. Cryst.* **2009**,

504, 164; g) R. Lartia, C. Allain, G. Bordeau, F. Schmidt, C. Fiorini-Debuisschert, F. Charra, M.-P. Teulade-Fichou, *J. Org. Chem.* **2008**, *73*, 1732.

25. a) D. Cvejn, E. Michail, I. Polyzos, N. Almonasy, O. Pytela, M. Klikar, T. Mikysek, V. Giannetas, M. Fakis, F. Bureš, *J. Mater. Chem. C* **2015**, *3*, 7345; b) D. Cvejn, E. Michail, K. Seintis, M. Klikar, O. Pytela, T. Mikysek, N. Almonasy, M. Ludwig, V. Giannetas, M. Fakis, F. Bureš, *RCS Adv.* **2016**, *6*, 12819.
26. a) X. Li, Y.-A. Son, Y.-S. Kim, S.-H. Kim, J. Kun, J. Shin, *J. Nanosci. Nanotechnol.* **2012**, *12*, 1497; b) C. Lambert, W. Gaschler, E. Schmälzlin, K. Meerholz, C. Bräuchle, *J. Chem. Soc., Perkin Trans*. **1999**, 577; c) R. Misra, R. Maragani, P. Gautam, S. M. Mobin, *Tetrahedron Lett.* **2014**, *55*, 7102.
27. H. Hartmann, S. Scheithauer, *J. Prakt. Chem.* **1969**, *311*, 827.
28. M. Blanchard-Desce, V. Alain, P V. Bedworth, S. R. Marder, A. Fort, C. Runser, M. Barzoukas, S. Lebus, R. Wortmann, *Chem. Eur. J.* **1997**, *3*, 1091.
29. a) I. M. Downie, E. J. Martyn, H. Heaney, K. F. Shuaibar, *Tetrahedron* **1993**, *49*, 4015; b) J. A. Clarke, O. Meth-Cohn, *Tetrahedron Lett.* **1975**, *52*, 4705.
30. F. Texier-Boullet, A. Foucaud, *Tetrahedron Lett.* **1982**, *23*, 4927.
31. M. S. Yosubov, E. N. Tveryakova, E. A. Krasnokutskaya, I. A. Perederyna, V. V. Zhdankin, *Synth. Commun*. **2007**, *37*, 1259.
32. J. Shao, S. Ji, X. Li, J. Zhao, F. Zhou, H. Guo, *Eur. J. Org. Chem.* **2011**, 6100.
33. a) J. J. La Clair, *J. Am. Chem. Soc*. **1997**, *119*, 7676; b) A. Auffrant, B. Jaun, P. D. Jarowski, K. N. Houk, F. Diederich, *Chem. Eur. J*. **2004**, *10*, 2906.
34. a) D. B. Dess, J. C. Martin, *J. Org. Chem.* **1983**, *48*, 4155; b) V. V. Zhdankin, P. J. Stang, *Chem. Rev*. **2008**, *108*, 5299.
35. C. W. Bird, *Tetrahedron* **1986**, *42*, 89.
36. A. A. Isse, A. Gennaro, *J. Phys. Chem. B* **2010**, *114*, 7894.
37. F. Terenziani, C. Le Droumaguet, C. Katan, O. Mongin, M. Blanchard-Desce, *ChemPhysChem* **2007**, *8*, 723.
38. Gaussian 09, Revision D.01, D. J. Fox *et* al., Gaussian, Inc., Wallingford CT, **2013**.
39. a) M. Qin, C. Wang, F. Zhao, P. Zeng, P. Cai, M. Fang, G. Lu, *Opt. Eng*. **2015**, *54*, 057101; b) L. M. Ganesan, W. Wirges, A. Mellinger, R. Gerhard, *J. Phys. D: Appl. Phys*. **2010**, *43*, 015401.
40. M. Makowska-Janusik, E. Gondek, I. V. Kityk, J. Wisla, J. Sanetra, A. Danel, *Chem. Phys*. **2004**, *306*, 265.

41. I. V. Kityk, A. Majchrowski, J. Zmija, Z. Mierczyk, K. Nouneh, *Cryst. Growth Des*. **2006**, *6*, 2779.
42. S. Tkaczyk, M. Galceran, S. Kret, M. C. Pujol, M. Aguiló, F. Díaz, A. H. Reshak, I. V. Kityk, *Acta Mater.* **2008**, *56*, 5677.
43. ArgusLab 4.0, Mark A. Thompson, Planaria Software LLC, Seattle, WA. http://www.arguslab.com.
44. MOPAC2012, J. J. P. Stewart, Stewart Computational Chemistry, version 13.084W, webpage: http://OpenMOPAC.net.
45. a) M. G. Vivas, D. L. Silva, J. Malinge, M. Boujtita, R. Zaleśny, W. Bartkowiak, H. Ångren, S. Canuto, L. De Boni, E. Ishow, C. R. Mendonca, *Sci. Rep.* **2014**, *4*, 04447; b) P. Hrobárik, V. Hrobáriková, I. Sigmundová, P. Zahradník, M. Fakis, I. Polyzos, P. Persephonis, *J. Org. Chem.* **2011**, *76*, 8726; c) Y.-P. Tian, L. Li. Y.-Z. Zhang, J.-X. Yang, H. Zhou, J. Wu, P. Sun, L. Tao, Y. Guo, C.-K. Wang, H. Xing, W. Huang, X.-T. Tao, M.-H. Jiang, *J. Mater. Chem.* **2007**, *17*, 3646.